Mathematical Modeling of Lactate Metabolism in the Brain

Milad Soltanzadeh

A Thesis

in

The Department

of

Electrical and Computer Engineering

Presented in Partial Fulfillment of the Requirements

for the Degree of

Master of Applied Science (Electrical and Computer Engineering) at

Concordia University

Montréal, Québec, Canada

November 2021

CONCORDIA UNIVERSITY

School of Graduate Studies

This is to certify that the thesis prepared

By: **Milad Soltanzadeh**

Entitled: **Mathematical Modeling of Lactate Metabolism in the Brain**

and submitted in partial fulfillment of the requirements for the degree of

Master of Applied Science (Electrical and Computer Engineering)

complies with the regulations of this University and meets the accepted standards with respect to originality and quality.

Signed by the Final Examining Committee:

_____ Chair
Dr. William E. Lynch

_____ External Examiner
Dr. Jean-Paul Soucy (McGill University)

_____ External Examiner
Dr. Solenna Blanchard (Université de Rennes 1)

_____ Examiner
Dr. Nawwaf Kharma

_____ Supervisor
Dr. Habib Benali

Approved by _____
Dr. Yousef Shayan, Chair
Department of Electrical and Computer Engineering

_____ 2021

_____
Dr. Mourad Debbabi, Dean
Faculty of Engineering and Computer Science

Abstract

Mathematical Modeling of Lactate Metabolism in the Brain

Milad Soltanzadeh

It is well established that the primary substrate for brain energy metabolism is glucose, but accumulating evidence suggests that lactate can also be considered as an energy substrate for the brain. Additionally, it has been shown that lactate is linked to memory, epilepsy, and traumatic brain injury, which emphasizes the importance of lactate. Considering the effects of lactate and the complexity of imaging its dynamics in neurons and glial cells, researchers are motivated to explore lactate dynamics using mathematical modeling. In this thesis, we propose a new mathematical model for brain lactate exchanges which includes four compartments. In summary, our model consists of four ordinary differential equations explaining interactions between neuronal, astrocytic, capillary, and extracellular space compartments. We simulate this model to assess its abilities to reproduce different qualitative behaviors of lactate dynamics in the brain. These scenarios include increased lactate transport to the brain due to physical exercise and increased lactate production inside neurons and astrocytes. Also, parameter estimation becomes crucial for these types of models due to its effect on the model's ability to reproduce correct physiological and pathological behavior of the brain. Some parameters can be determined from the experiments in the literature. However, for some of them, there is not a consensus over the values. In this case, an optimization can be done to determine the parameters. In this thesis, we fixed the parameter values for lactate transport and optimized the lactate production and consumption parameters.

Acknowledgments

I would like to express my sincere gratitude to my supervisor Dr. Habib Benali. I appreciate his scientific advice, technical assistance, insightful suggestions, and financial support throughout my research. I am very grateful for his continuous support during my studies. I also wish to thank Dr. Solenna Blanchard for her assistance, comments, and methodological and scientific guidance. I would like to thank my thesis committee Drs. William Lynch, Jean-Paul Soucy, Nawwaf Kharma, Solenna Blanchard and Habib Benali for their constructive discussions and suggestions. I would like to acknowledge that this work was supported by NSERC CRC grant NC0981 and Faculty Research Support by Concordia University.

I would like to thank my wife, Fatemeh, for her unconditional love and companionship during the past years. I wish to thank my father, Majid, and my mother, Mehrangiz, for their strong support since my childhood. I am grateful to my father-in-law, Asghar, for his belief in my abilities and his continuous support. I also had great pleasure of working with my colleagues in Bhealthy Age Lab and I appreciate their useful discussions and suggestions.

Contents

List of Figures

List of Tables

Chapter 1

Introduction

This chapter provides a summary of key components of the thesis. A comprehensive literature review is presented in chapters 2 and 3.

1.1 Mathematical Modeling of Brain Metabolism

The brain is an organ with high energy demands compared to other organs in the human body. Brain energy needs are primarily provided through glucose, but lactate and ketone body are alternative sources of brain energy in certain circumstances [5]. Energy substrates are transported to the brain by blood vessels. They are utilized in case of energy demand in which cerebral blood flow (CBF) increases to supply more nutrients to the activated brain regions [6, 1].

Due to the emphasis on the importance of lactate over the past years and the lack of direct access to the physiological processes in the lower level, mathematical models are proposed to capture the possible mechanisms of lactate metabolism in the brain. These models are utilized to provide mathematical evidence for a specific hypothesis, study intermediary variables involved in a physiological process, and predict the system's behavior, which can help design experiments.

Over the past years, some models for brain metabolism have been proposed, but new models are required to take into account our updated physiological knowledge. These updates are reflected in the compartmentalization, equations, and parameters of the models. Also, some of these models did not consider the effect of parameters on their conclusion on the lactate behavior in the brain. They

also have parameters that are biased toward a specific direction of lactate uptake or release, such as astrocyte-neuron lactate shuttle.

1.2 Contribution of the Thesis

This thesis proposes a mathematical model for lactate metabolism in the brain based on the current physiological literature. This model consists of four ordinary differential equations (ODEs), each tracking lactate concentration in one of the four compartments considered for this lactate model. These compartments include pyramidal neuron, extracellular space, astrocyte, and capillary. We analyze the possible behaviors of the model in resting and its transients to different states by varying a few parameters. We also simulate the equations over time to test the output of the model in different scenarios. We specifically test the effect of artery lactate on neuronal lactate metabolism in the energy demand situation.

1.3 Organization of the Thesis

In chapter 2, a more detailed review on the brain metabolism of lactate is presented. Chapter 3 reviews concepts of mathematical modeling and optimization. Then a review of other models of brain metabolism is included. In chapter 4, we present the proposed model and then we include results of optimization in resting and simulation of different scenarios. Finally, chapter 5 will summarize the findings and future work.

1.4 Publications

- Soltanzadeh M, Blanchard S, Benali H. A computational model for brain lactate exchanges in neuro-glio-vascular coupling. Organization for Human Brain Mapping (OHBM); 2021; Online.
- Soltanzadeh M, Benali H, Blanchard S. A physiologically-based computational model to study brain lactate exchanges. Organization for Human Brain Mapping (OHBM); 2020; Online.

- Soltanzadeh M, Blanchard S, Benali H. Optimization study of a new computational model for brain lactate exchanges at rest. Organization for Human Brain Mapping (OHBM); 2020; Online.
- A journal article is in preparation including the model and its analysis and will be submitted soon to the Journal of Cerebral blood flow and Metabolism.

Chapter 2

Physiological Background

2.1 Introduction

In this chapter, we first briefly introduce neurons and astrocytes and their interactions, and then elaborate on brain metabolism. Finally, we review mechanisms of lactate transport and production and its potential roles in the brain.

2.2 Brain Compartments and Energy Metabolism

Main types of brain cells are *glial cells* and *neurons*. Neurons are considered the main components of the brain. Different networks of neurons are connected, and the generated action potential is propagated along their axons. The action potential is an electric signal that is created by the imbalance in the equilibrium of ions between extracellular and intracellular space. This signal is created when the neurons are stimulated more than a certain threshold. This is called *firing* of neurons. When the signal reaches the point where two neurons are connected and created a *synapse*, *neurotransmitters* are released in the joint area that is called *synaptic cleft*. These neurotransmitters will activate receptors in the following neuron, and the action potential continues to move along the next neuron's axon [7].

Neurons are divided into different categories based on their functionality, structure, shape, and axon length. In a classification, neurons are classified as excitatory or inhibitory. Excitatory neurons

release neurotransmitters, which causes the receiving neuron to increase the potential and get closer to the firing voltage threshold of the neurons. If enough excitatory signals arrive at a neuron, the action potential is generated. Contrary to the excitatory neurons, inhibitory ones reduce the potential and inhibit the postsynaptic potential in the subsequent neuron. So, they decrease the chance of firing in the receiving neuron. The most numerous type of excitatory neurons are pyramidal neurons and they mainly release glutamate as neurotransmitter, so they are called glutamatergic neurons. On the other hand, inhibitory neurons are GABAergic neurons as they release gamma-aminobutyric acid (GABA) as neurotransmitter [7, 5].

Glial cells mainly include astrocytes, microglia, Schwann cells, and oligodendrocytes. Glial cells are the most abundant cells in the brain, and they are known as the supporters of neurons. Contrary to the neurons, they do not produce action potential nor form dendrites. Microglial cells are part of the immune system in the central nervous system. Schwan cells and oligodendrocytes form myelination around axons, which boosts the propagation of action potential. The difference between Schwann cells and oligodendrocytes is that the former act in the peripheral nervous system and the latter in the central nervous system [7].

Astrocytes interact with the neurons in many ways, including synapse formation, uptaking neurotransmitters from the synaptic cleft, regulation of k^+ ion, and nourishing neurons' energetic demands. Astrocytes' end-feet surround blood vessels and uptake nutrients such as glucose and lactate [7]. For instance, if glutamate uptake by the astrocytes stops working, the concentration of glutamate in the extracellular space increases and leads to the death of neurons. This phenomenon is called neurotoxicity [8].

2.2.1 Glycolysis

Glucose is the main energy substrate of the brain, which produces Adenosine Triphosphate (ATP) due to a metabolic reaction network called glycolysis. Glycolysis is the process in which pyruvate is produced from glucose. This process involves several intermediary reactions and enzymes as shown in a simplified format in Figure 2.1 and a more detailed format in Figure A.1 [9, 4, 5].

Then pyruvate has two ways to be converted. First, in the presence of enough oxygen, it can

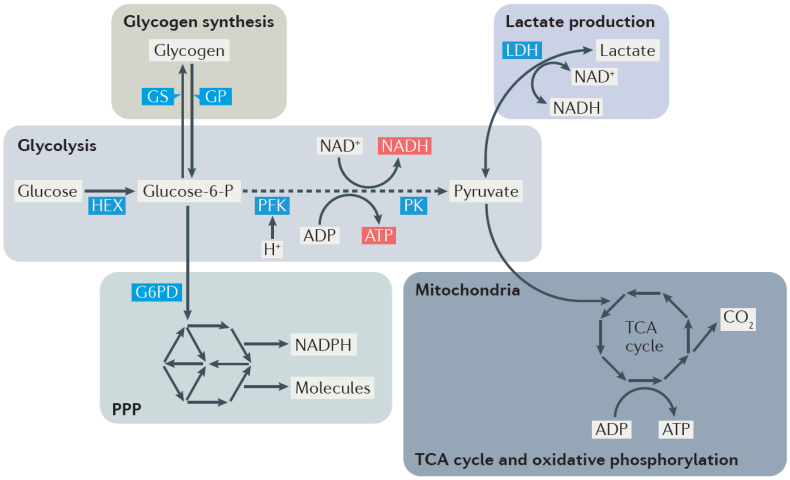

Figure 2.1: This figure shows different pathways of glucose utilization and provision. It shows oxidative phosphorylation and aerobic and anaerobic glycolysis. Glucose can also be derived from glycogen. (taken from [1])

be oxidized to water and carbon dioxide and produce ATP. In mitochondria, pyruvate is oxidized by entering the tricarboxylic acid cycle (TCA cycle), also known as the Krebs cycle. As a second option, it can produce lactate with the help of the lactate dehydrogenase (LDH) enzyme. The former is called *oxidative phosphorylation*. The latter pathway, producing lactate, happens when there is not sufficient oxygen delivery to fully oxidize glucose [5]. In this case, this pathway is called *anaerobic glycolysis*. In some circumstances, reduction of pyruvate to lactate can also happen when the oxygen level is normal and is called *aerobic glycolysis*. Aerobic glycolysis can happen in cells such as astrocyte and cancer cells [1]. Even though oxidative metabolism results in more ATP production (30 ATP molecules vs. 2 molecules in glycolysis), but glycolysis happens at a faster rate. Therefore, it is suited to the sudden energy demands of Na^+/K^+-ATPase. Aerobic glycolysis varies over different brain regions that can be due to the differences in the percentage of non-neuronal cells [10, 5]. In this thesis, we are focused on modeling only lactate dynamics.

Most shreds of evidence are compatible with the fact that glycolytic activity and lactate utilization happens in the glutamatergic neurons and not in the GABAergic neurons [1, 11]. Chatton et al. [12] studied the relationship between GABA uptake and metabolic activity in the astrocytes. They did not find an association between increased glycolytic activity and GABA release by the neurons. Based on these pieces of evidence, we only consider pyramidal neurons in our model.

2.3 Lactate

Lactate is a substrate produced and metabolized in the human body, especially in the muscles during physical exercise or in the brain. For instance, muscles produce lactate during physical exercise, and then lactate is transported to the heart to be used as an energy substrate. In addition to the energetic role of lactate, studies have found other functions for lactate. According to [13], lactate is effective in retrieving memory in rats, while in another study, Sada et al. [14] suggested that inhibiting lactate production inside the brain can potentially reduce epileptic seizures. In the next sections, we will introduce some of the lactate contributions in more detail.

2.3.1 Lactate Contributions

Energy Substrate

Lactate was initially considered the waste product of physical exercise with no specific role in the brain, but this view has changed over the past decades. First, it was shown that lactate could be metabolized by the neurons [15, 16] and then Pellerin et al. [17, 18] provided evidence in favor of glutamate uptake and lactate release by the astrocytes upon activation. They suggested a mechanism in which astrocytes produce lactate from glucose during stimulation to provide energy substrates for the neurons. They called it the astrocytes-neuron lactate shuttle, which will be introduced in the subsequent sections.

In a later study, Wyss et al. [15] provided in-vivo evidence concerning the energetic roles of lactate. Their results suggested that neurons preferably consume lactate rather than glucose in the presence of both substrates, which can help the neuronal activity to be maintained despite a drop in glucose levels.

Epilepsy

Epileptic seizures are associated with the sudden and synchronized activity of neurons. An essential aspect of seizures is their high energy demands which can be met by lactate and glucose. So, one mechanism to suppress seizures is to inhibit the energy supply to neurons [19].

In a series of experiments, Sada et al. [14] investigated the effect of inhibiting lactate production on controlling epileptic seizures. First, they hyperpolarized neuron membrane by using β-hydroxybutyrate (a ketone body) and removal of glucose. Then by administration of lactate, hyperpolarization reversed, meaning that lactate can be converted to pyruvate resulting in ATP production. They also inhibited LDH to stop lactate production, and they observed that it causes membrane voltage to decrease. Altogether, their results propose that inhibition of LDH could be helpful to suppress seizures as it reduces membrane potential and decrees the chances of neurons to fire.

Plasticity and Memory

In a study by Suzuki et al. [13], they investigated the effect of inhibiting glycogen-derived lactate production inside astrocytes on memory consolidation in rats. They showed that this inhibition of lactate production impaired rat's memory in avoiding a dark room with an electric shock. Figure 2.2 displays the experimental procedure and the results. In addition, in some studies deficits in the expression of specific lactate transporters resulted in impaired memory [1].

Exercise and Lactate

Some studies proposed lactate metabolism during exercise as an alternative for glucose [20]. Rasmussen et al. [21] analyzed several published experiments that investigated arterio-venous lactate concentration differences and concluded that a net lactate uptake by the brain during exercise. Quistorff et al. [22] proposed lactate as an alternative energy substrate during exhaustive exercise by analyzing cerebral metabolic ratio (CMR). CMR is defined as the cerebral molar uptake ratio of $\frac{oxygen}{glucose+0.5lactate}$.

Matsui et al. [20] examined the role of glycogen-derived lactate in fueling the brain during exercise. Their findings suggest that inhibiting glycogen phosphorylation reduces lactate and, as a result, hippocampal ATP concentration at the exhaustion level of physical exercise. They also stated that slighter levels of exercise increases levels of monocarboxylate transporters in the brain.

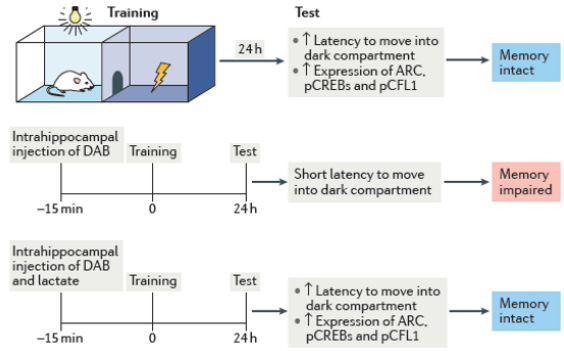

(a) Experimental protocol

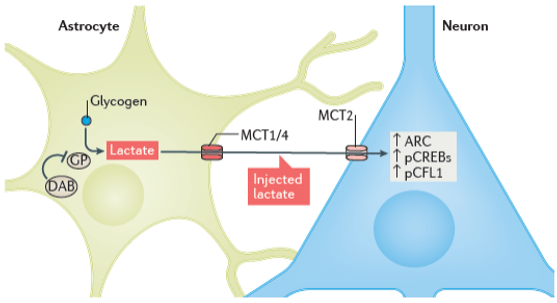

(b) Proposed mechanisms

Figure 2.2: (a) This figure shows the experimental protocol to test for the effect of lactate on memory. The rat face an electric shock in the dark room and when they again tested it after 24 hours, it moved to the dark room with a delay. Inhibition of lactate production, removed this delay and then by injecting lactate the rat could do the task with a delay again after 24 hours. (b) This figure shows the proposed mechanism of lactate production and increased plasticity-related molecules (ARC, pCREBs, pCFL1) (taken from [1]).

Lactate as a Signaling Molecule

Lactate has also been proposed to have a signaling role in the brain. They act on the receptors called G-protein coupled receptors (GPR81), also known as HCAR1, and results in the production of cyclic adenosine monophosphate (cAMP) that regulates the metabolism of glucose inside neurons [1]. This signaling role of lactate can also change the excitability of neurons by acting on the N-Methyl-D-aspartate (NMDA) receptors and intake of Ca2+ ions [23].

2.3.2 Monocarboxylate Transporters

Lactate can be transported between brain compartments via monocarboxylate transporters (MCTs). There exist several isoforms of MCTs. MCT isoforms 1–4 are proton-coupled transporters that facilitate the transport of lactate and pyruvate across the membrane [24].

Main lactate transporters in the brain are MCT1, MCT2 and MCT4 [25, 26, 27]. Even though there are some discrepancies in the placement of these transporters in the brain but according to our literature review, there is an agreement about different types of the MCTs in the interface of different cells: ([28, 29])

(1) Neuron-Extracellular space interface (MCT2 representation)

(2) Astrocyte-Extracellular space interface (MCT4 representation)

(3) Astrocyte-Capillary interface (MCT1 representation)

They act in a bidirectional pathway and transport substrates by facilitated diffusion with co-transport of H+ ions [30]. Facilitated diffusion is a passive transport of metabolites without ATP consumption and is based on the gradient of the concentrations.

2.3.3 Lactate Production/Consumption

The LDH reaction mentioned in 2.2.1, is a bi-directional near-equilibrium reaction which produces lactate/pyruvate catalyzed by the LDH enzyme:

$$pyruvate + NADH \overset{LDH}{\rightleftarrows} lactate + NAD^{+} \tag{1}$$

There are different subtypes of LDH, but evidence suggests that LDH1 is more present in neurons while LDH5 is more found in the astrocytes. LDH1 favors lactate consumption to produce pyruvate. In contrast, LDH5, which favors lactate production [31]. Experimental studies suggest that neurons have more capacity to produce pyruvate, and astrocytes are adapted to produce more lactate [32].

In [2], they showed that more than 60% of neurons are lactate consumers while all the examined astrocytes were net lactate producers. The procedure included blocking MCTs to stop lactate transport to the cells and then measuring the lactate concentration dynamics. According to 2.3 those with

increasing dynamics are net producers that cannot export their surplus lactate. At the same time, those with decreasing curves are net consumers and, due to the blockade of MCTs, cannot import enough lactate. Few cells do not react to the MCT block.

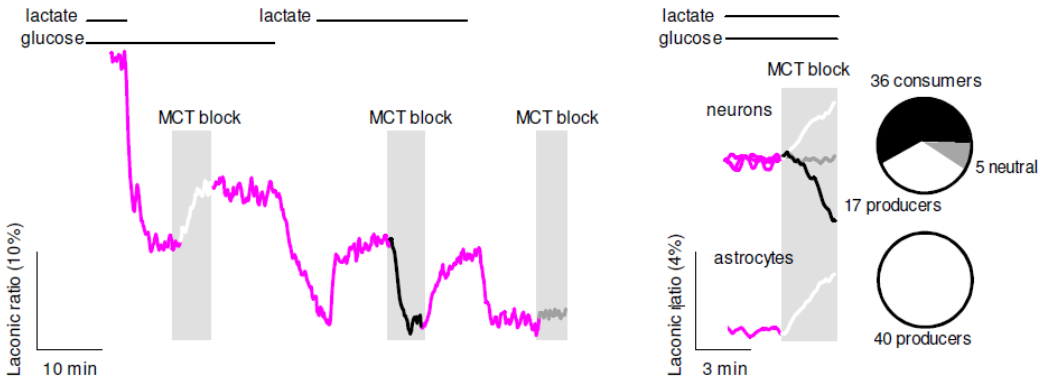

Figure 2.3: This figure illustrates an example response of neurons and astrocytes to lactate transporter (MCT) blockage. It shows if they are net producers or consumers of lactate (taken from [2])

2.3.4 Astrocyte-Neuron Lactate Shuttle (ANLS)

Pellerin et al. [18] first introduced the concept of lactate shuttling from astrocytes to neurons. They proposed this hypothesis based on an experiment in which astrocytes released lactate upon stimulation. Specifically, the release of lactate was triggered by glutamate uptake, a neurotransmitter released by the neurons when activated.

The existence of different transporters and enzymes in neurons and astrocytes has also reinforced the ANLS hypothesis. One example is what we mentioned in section 2.3.3 about the localization of LDH1 and LDH5 in neurons and astrocytes. Table 2 of [33] summarized evidences in favour of ANLS until 2004. Sotelo-Hitschfeld et al. [34] used a FRET sensor to evaluate the release of lactate from astrocytes in-vivo. They observed that increasing K^+ in the extracellular space cause membrane depolarization and observed a rapid fall in lactate concentration inside astrocytes. In addition, there is evidence that the baseline concentration of lactate inside astrocytes is higher than neurons, and it might enable them to create a gradient of lactate towards neurons [35].

On the other hand, there are pieces of evidence that emphasize the opposite direction (Neurons-Astrocyte Lactate Shuttle (NALS)) or at least suggest that astrocyte lactate is not necessary for neurons' metabolism [3]. NALS is also known as the classic view of lactate metabolism. Schurr and Payne [36] concluded that the share of astrocytic lactate from lactate consumption by neurons is low (15%). In another study, Based on the model proposed in [37] and using fMRS data, Mangia et al. [38] suggested that the glucose utilization capacity should be 12-fold higher to make ANLS possible.

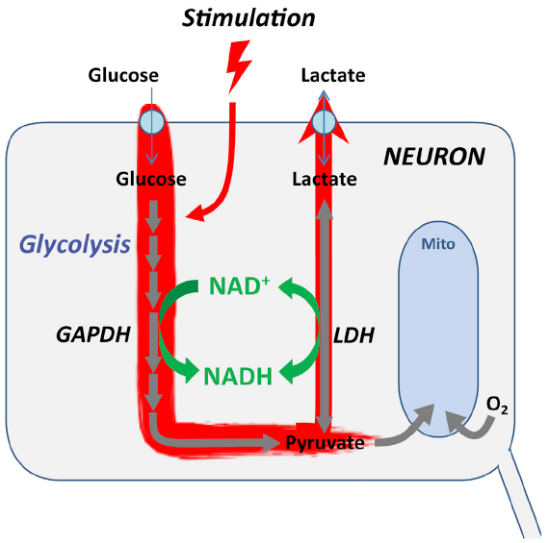

Figure 2.4: A proposed hypothesis that challenges ANLS view. Based on this hypothesis, glycolysis inside neurons is mainly responsible for providing energy substrate for the brain, and lactate produced in the neurons is possibly transported to the astrocytes (taken from [3])

Combining the two views on lactate shuttling, some researchers believe that there is a switch between these two different mechanisms [33, 39, 31]. [40] considered different roles for the aerobic and anaerobic glycolysis and suggested that the latter's role is more related to the maintenance of synaptic potentials. While [41] believes that the switch from glucose to lactate happens when neurons need more energy, [31] states that the neurons switch from glucose to lactate in some cases, like when the concentration of lactate is higher.

2.4 Challenges and Debates

There is a consensus over the importance of lactate, but there are still questions about the extent of its contributions and its mechanisms in the brain. One of the challenges is the direction of lactate shuttling (ANLS vs. NALS) that was addressed in section 2.3.4. In fact, the experiments and models aim to find if both directions exist and when the switch to each of them happens. This behavior can vary among species, different brain regions, and the level of activation. There are also questions about the role of blood lactate in the brain. It is well established that lactate uptake by the brain increases during physical exercise [21, 42]. However, researchers are still investigating how much this contributes to neuronal energy demands compared to glucose and brain lactate production. Understanding the mechanism of lactate contribution in physical activity can decipher the link between physical exercise, lactate, and the brain.

Additionally, there are questions about the end product of glycolysis. It is widely accepted that pyruvate enters mitochondria as the end product of glycolysis. But some observations and interpretations suggest lactate, not pyruvate, transport to mitochondria and then conversion of lactate to pyruvate with the help of mitochondrial lactate dehydrogenase (mLDH) enzyme [43]. In other words, lactate is not only the end product of anaerobic glycolysis but also the end product of aerobic glycolysis [42]. In a review by [6], they argued that based on their previous experiments and observations, considering lactate as the end product of glycolysis is a more consistent view. In chapter 4, we try to answer part of these questions from the perspective of our model.

Chapter 3

Mathematical Modeling of Brain Metabolism and Optimization

Mathematical modeling is widely used in neuroscience to simulate brain readouts and understand intermediary processes in the brain. Hodgkin and Huxley's model is a pioneer model that tried to model action potential propagation along axons. Another type of model called compartmental models assumes a "compartment" which is a well-mixed part of the system with no difference in the concentration of what we want to study. These types of models have been initially used in pharmacokinetics, and drug delivery studies [44]. Another important consideration in modeling is the level of abstraction. We can model a process in the level of a single cell, a region, or the whole brain as a unique system.

Even though, there has been a focus on neurons as the most important components of the brain, but in recent years, astrocytes have also grabbed the attention of neuroscientists. Their non-negligible role in the maintenance, metabolism, and regulation of neurons and synapses have made them an essential part of some recent computational models for the analysis of brain function. There are computational models that in addition to the neurons include astrocytes that recycle neurotransmitters and exchange other metabolites with the extracellular space. Some of these models can generate the local field potentials as an output [45]. Adding astrocytes can help to us decipher some hidden intermediary mechanisms and also we can observe the effect of them on the brain data such

as EEG or fMRI.

This chapter introduces mathematical modeling of chemical reactions and reviews other proposed mathematical models for brain metabolism with a focus on lactate and optimization used for model's parameters estimation.

3.1 Mass Action Law

According to this intuitive law, rate of a reaction is determined in proportion to the product of the concentrations of the reactants that take part in the reaction [46]. This gives us a quantitative model to determine the reaction velocity and final concentrations starting with a specific initial condition. The following sections will present applications of this law with a few examples.

3.1.1 Chemical Reactions rate

For a basic reaction in which A is converted to B in an uni-directional way, we can derive the reaction rate as follows:

$$A \xrightarrow{k_1} B \quad so, \quad \dot{B} = rate = k_1[A] \tag{2}$$

In which $\dot{B}$ is the time derivative of the product that shows the rate at which the reaction is happening and k_1 is known as the **rate constant**. This reaction rate is written based on the law of mass action [47]. For more complex settings the reaction rate will become [46, 48]:

$$\begin{cases} A + B \xrightarrow{k_1} C \quad so, \quad \dot{C} = k_1[A][B] \\ 2D \xrightarrow{k_2} E \quad so, \quad \dot{E} = k_2[D]^2 \end{cases} \tag{3}$$

according to these examples, the rate for products is positive, while for reactants, we use a negative sign because they decay over time. Solving these differential equations, we can obtain the transition and steady state concentrations of a reactant or product.

Enzymatic reactions

In enzymatic reactions, the enzyme affects the reaction rate, but it is present without changes at the equilibrium. In the case of enzyme-substrate reactions, the enzyme (E) forms an enzyme-substrate complex (ES) which then is converted to the product (P) (Equation 4).

$$E + S \underset{k_{-1}}{\overset{k_1}{\rightleftarrows}} ES \overset{k_2}{\rightarrow} P + E \tag{4}$$

Writing reaction rates at each step gives us a system of ODEs (Equation 5). Solving this system enables us to obtain the rate at which product is formed as a function of rate constants and substrate concentration.

$$\begin{cases} [\dot{S}] = -K_1[S][E] + K_{-1}[ES] \\ [\dot{E}] = -K_1[S][E] + K_{-1}[ES] + K_2[ES] \\ [\dot{ES}] = K_1[S][E] - K_{-1}[ES] - K_2[ES] \\ [\dot{P}] = K_2[ES] \end{cases} . \tag{5}$$

In equation 5, [X] refers to the concentration of species involved in the reaction and K_i is the rate constant for each direction. To solve this ODE system, we make two simplifying assumptions [46]:

(1) Total enzyme concentration is constant. So:

$$[E_{total}] = [E] + [ES] \rightarrow [\dot{E_{total}}] = 0 \tag{6}$$

(2) Substrate concentration is considerably higher than enzyme concentration ($[S] >> [E_{total}]$)

The first assumption leads to the following ODE system:

$$\begin{cases} [\dot{S}] = -K_1[S]([E_{total}] - [ES]) + K_{-1}[ES] \\ [\dot{ES}] = K_1[S]([E_{total}] - [ES]) - K_{-1}[ES] - K_2[ES] \\ [\dot{P}] = K_2[ES] \end{cases} . \tag{7}$$

The second assumption results in the fast equilibrium of enzyme complex, a situation known as quasi steady state. So we can set its time derivative equal to zero:

$$0 = -k_{-1}[ES]_{qss} + k_1[S]([E_{total}] - [ES]_{qss} - k_2[ES]_{qss}) \tag{8}$$

meaning that $[ES]_{qss} = \frac{k_1[E_{total}][S]}{K_{-1}+k_2+k_1[S]}$.

By doing this, we can reduce the problem to a 2-D ODE problem:

$$\begin{cases} [\dot{S}] = -\frac{k_2 k_1[E_{total}]S}{k_{-1}+k_2+k_1 S} \\ [\dot{P}] = \frac{k_2 k_1[E_{total}]S}{k_{-1}+k_2+k_1 S} \end{cases} . \tag{9}$$

Based on equation 9 and combining parameters we can obtain the conversion rate of S to P as:

$$rate = V_{max}\frac{S}{K_M + S} \tag{10}$$

In which $V_{max} = k_2[E_{total}]$ and $k_M = (k_{-1} + k_2)/k_1$

Equation 10 is called **Michaelis-Menten** equation and can describe behavior of many chemical reactions. In this equation V_{max} is the *maximum reaction velocity* happening in saturation while K_M is the concentration at which the reaction velocity is $V_{max}/2$. K_M is called *Michaelis constant* [47]. Figure 3.1 represents a typical Michaelis-Menten curve and its parameters.

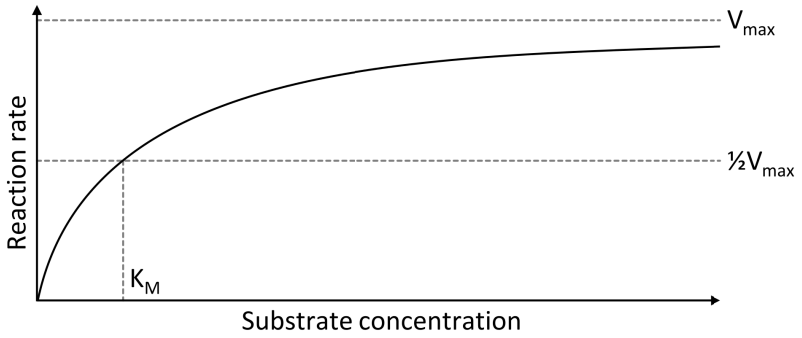

Figure 3.1: An illustration of the Michaelis-Menten kinetic equation and the parameters V_{max} and K_M. [1]

[1] from wikipedia.org

Similar to this analysis, one can obtain rates for other types of reactions that are more complicated. Suppose that the product can reversibly be converted to the substrate:

$$E + S \underset{k_{-1}}{\overset{k_1}{\rightleftarrows}} ES \underset{k_{-2}}{\overset{k_2}{\rightleftarrows}} P + E \tag{11}$$

In this case according to [48], the reaction velocity can be written as:

$$rate = e_0 \frac{k_1 k_2 s - k_{-1} k_{-2} p}{k_1 s + k_{-2} p + k_{-1} + k_2} \tag{12}$$

In facilitated diffusion, we have a carrier protein that binds the substrate and transports it across the membrane. This phenomenon has similar properties to a reversible catalyzed reaction, except that product is the transported substrate without a chemical change. With some manipulations, the reaction rate for facilitated diffusion is written as [46]:

$$rate = \frac{V_{m1}[S_1]/K_{m1} - V_{m2}[S_2]/K_{m2}}{1 + [S_1]/K_{m1} + [S_2]/K_{m1}} \tag{13}$$

S_1, S_2 represent the substrate inside and outside of the membrane. $V_{m1} = [E_{total} k_2], V_{m2} = [E_{total} k_{-1}]$ are the maximum transport rates and $K_{m1} = (k_{-1}+k_2)/k_1, K_{m2} = (k_{-1}+k_2)/k_{-2}$ are the Michaelis constants for each side of the membrane. This is also known as **reversible Michaelis-Menten** equation.

3.2 Review of Lactate Models

In this section, we will briefly review some of the brain metabolism models with a more detailed explanation of the Aubert-Costalat reduced model proposed in [49].

3.2.1 Aubert-Costalat Model

In 2005, Aubert and Costalat [49] proposed a reduced model for lactate based on their previous works since 2002 on the brain metabolism modeling [50, 51].

In [49], they considered lactate dynamics and interactions between two compartments: capillary

and extracellular space. They validated their results by fitting the output of their model to the experimental data in the extracellular space published in [52]. The following ODEs modeled the dynamics of lactate:

$$\begin{cases} V_e \dot{Lac}_e = J_{mb} - J_{Diff} - J_{BBB} \\ V_c \dot{Lac}_c = J_{Cap} + J_{BBB} \end{cases} \tag{14}$$

Where, J_{mb} refers to the superposition of the rate of lactate release/uptake from/by neurons and astrocytes while J_{Diff} represents the rate of lactate diffusion. J_{BBB} is the rate of lactate transported through the blood-brain barrier (BBB). Finally, J_{Cap} shows the contribution of blood flow to the changes in capillary lactate concentration [49]. V_e and V_c are volume fractions of the extracellular space and capillary, respectively. Expanded equations for these intermediate variables are written in equation 15.

$$\begin{cases} J_{tissue} = J_{mb} - J_{Diff} = J(t) + \beta(Lac_{e0} - Lac_e) \\ J_{BBB} = T_{max}(\frac{Lac_e}{K_t + Lac_e} - \frac{Lac_c}{K_t + Lac_c}) \\ J(t) = \begin{cases} (1+\alpha_{Ji})J_0 \quad for \quad 0 \le t \le t_i \\ (1+\alpha_J)J_0 \quad for \quad t_i + t_J \le t \le t_{end} \\ J_0 \quad for \quad t < t_{start} \quad or \quad t \ge t_{end} + t_J \end{cases} \end{cases} \tag{15}$$

In equation 15, T_{max} is the maximum reaction velocity and K_t is the Michaelis constant for the lactate exchange between capillary and extracellular space. Lac_{e0} is the extracellular lactate concentration at rest. α_x are the scaling parameters for the input $J(t)$. $J(t)$ linearly increases between t_i and $t_i + t_J$ while linearly decreases in the interval of t_{end} and $t_{end} + t_J$. Table 3.1 contains the parameter values and their units.

Table 3.1: Parameter set for the simulation of reduced Aubert-Costalat model

V_e	V_c	β	J_0	T_{max}	K_t	CBF_0	Lac_a	Lac_{e0}	Lac_{c0}
-	-	s^{-1}	$mM.s^{-1}$	$mM.s^{-1}$	mM	s^{-1}	mM	mM	mM
0.2	0.0055	0.001	0.001	0.0061	3.5	0.01	0.3	1.19	0.35
α_F	t_F	α_{Ji}	t_i	α_J	t_J	t_{end}	t_{start}		
-	s	-	s	-	s	s	s		
0.8	5	-0.8	18	4.73	5	190	120		

They simulated the model by setting up a single and repetitive increase of CBF and increased neuronal activity. neuronal activity is increased by changing J_{tissue}. As visualized in Figure 3.2, we re-simulated their single stimulation scenario. They also examined the effect of pH on the dynamics and found no considerable effect.

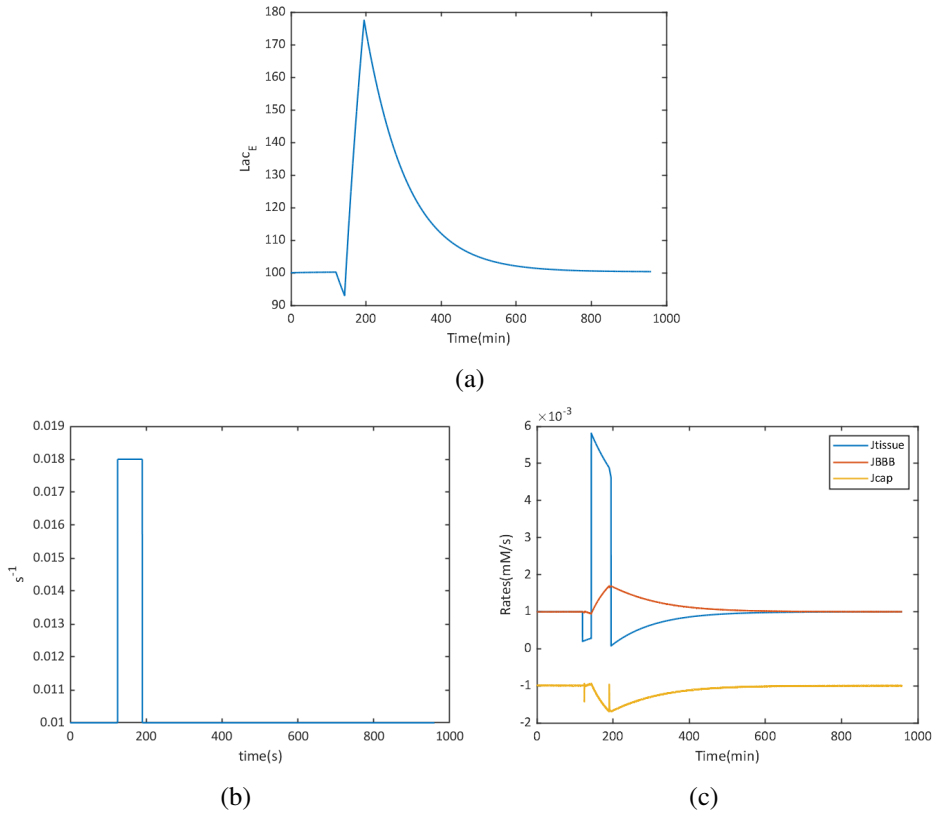

(a)

(b)

(c)

Figure 3.2: Simulation of the Aubert-Costalat reduced model. (a) Represents extracellular lactate concentration with an initial dip. (b) CBF changes in a 70-second period that given as an input to the model. (c) Dynamical transitions of the intermediary variables including J_{tissue}, J_{cap}, and J_{BBB}.

Figure 3.2a shows dynamics of extracellular lactate concentration obtained by 70-s increase in CBF amplitude and a specific form for $J_{tisssue}$ as shown in Figure 3.2c. Their model was able to reproduce the experimental results of [52]. They specifically created the initial dip in the extracellular lactate concentration upon stimulation using appropriate parameters and inputs. This initial dip has been one of the most important experimental evidence of neurons' need to lactate upon stimulation.

3.2.2 Simpson Model

Considering six compartments of serum, endothelial cells, basal lamina, interstitium, astrocytes, and neurons, Simpson et al. [37] developed a model to investigate lactate and glucose dynamics. An essential aspect of the Simpson model is that their simulations support the release of lactate by the neurons through the extracellular space and NALS hypothesis. They state that the astrocyte's capacity to transfer lactate is not enough to make it the primary lactate producer and transporter. Similar to Aubert-Costalat, they also optimized the model to reproduce experimental data in [52].

Jolivet et al. [53], reviewed recent models of that time, such as the Simpson model. Specifically, they computed the ratio of glucose uptake in neurons and astrocytes for this model. According to their results ratio of astrocyte glucose uptake is 0.132 and decreases to 0.018 in activation mode. They argued that this is not in agreement with the physiological and modeling literature in which the astrocytes mainly capture glucose, and it increases during activation . In response to this commentary, Mangia et al. [54] debated the claim that more glucose uptake by the astrocytes is a reason that the Simpson model did not predict ANLS. They argued that even by increasing this ratio, they still observe NALS. They also mentioned that it had been shown that glycolytic activity in both astrocytes and neurons increases upon activation [55]. In a later study, a modified Simpson model proposed that could reproduce ANLS behavior under some conditions [38].

3.2.3 Cloutier Model

Cloutier et al. [56] proposed this model as an extension to the metabolic models in [50, 51] by adding glycogen dynamics. They modeled the dynamics of several metabolites and intermediary processes involved in brain metabolism. Regarding lactate, in Cloutier's model, neurons only interact with the extracellular space and can produce and consume lactate. However, astrocytes can also exchange lactate with the capillary. Equations and parameters for the LDH and MCT kinetics in this model are taken from [50, 51]. In the first scenario, they simulated a 5-minute sharp stimulation which caused more lactate production inside astrocytes and more lactate consumption inside neurons. In their model at the baseline, neurons are net lactate consumers, and their results support ANLS.

3.2.4 Rangel Model

In a recent model proposed in [57] they explored the link between hemodynamics, metabolism, and electrical activity of the brain in resting and activation. In their model, astrocytes act as an intermediary compartment between blood vessels and neurons, and all compartments interact with the extracellular space. They modeled the rates for reactions using Michaelis-Menten kinetics equations, and they defined arterial lactate and CBF as inputs to the model.

Results that are shown in Figures 4 and 5 of [57] indicate an increase in the lactate production inside neurons upon increased activation and a switch to pyruvate production in the astrocytes upon the start of activation. These results are not in favor of the ANLS hypothesis. Additionally, lactate transfer from extracellular space to neurons is reversed during activation, which supports NALS.

3.2.5 Other Models

There are other models in the literature that dealt with the various physiological hypothesis and different analysis techniques. In a study by Somersalo et al. [11], they reviewed known metabolic models and proposed a probabilistic approach for analyzing their previous developed model [58]. in this method, instead of fixing the model's parameters, a probability distribution is assumed around the flux rates and reaction kinetics. The mean of this distribution is chosen based on the literature. Their results, as depicted in Figure 7 of [11], show that the ratio of glucose compartmentalization between neurons and astrocytes is crucial in determining the direction of the lactate shuttle. Later they applied the Markov chain Monte Carlo (MCMC) method for uncertainty quantification in a spatio-temporal model of brain metabolism [55].

Patsatzis et al. [59] analyzed a computational model for lactate kinetics using the computational singular perturbation (CSP) method. This algorithm can distinguish between the parameters based on their contribution to the fast/slow dynamics. Therefore, CSP can quantify the influence of a parameter or metabolite on the temporal evolution of the system. They analyzed the lactate model proposed in [37] and [38]. They concluded that lactate transport between astrocytes and interstitium determines whether ANLS will emerge from a model or NALS. In fact contribution of this factor to the fast dynamics results in ANLS and vice versa. Jolivet et al. [60] proposed a multi-scale

model to simulate links between excitation and metabolism in the neuro-glio-vascular coupling. From the lactate perspective, their equations and compartmental organization are the same as those in [56, 51].

3.2.6 Discussion and Conclusion

Even though the introduced models might differ in compartmentalization, equations, parameters, and analysis methods, they have common terms. For instance, the models proposed by Cloutier [56] and Jolivet [60], are both the same as the model proposed in [51] in terms of equations and some parameter values.

One important consideration is that most of these introduced models pay less attention to the variability of parameters and how this can affect their conclusions. Additionally, there is usually more focus on the simulation of the model in an activation period and the resting state condition is fixed. At the same time, there are also variabilities in resting that affect the activation results as well.

The Aubert-Costalat reduced model's result is fitted to the data by Hu and Wilson [52] and it can precisely reproduce the initial dip in the extracellular lactate concentration. This result is promising and shows the model's physiological capabilities. However, looking back at Figure 3.2c, we see that this is partly due to how they chose their inputs. They added an initial dip to J_{tissue}, which causes the demand in the beginning and results in a good fitting.

In addition, it should be noted that fitting the results does not guarantee the validity of all the conclusions. For instance, When we compare Simpson and Aubert-Costalat model, we see that both models fitted their results to the experimental data by Hu and Wilson. Nevertheless, they have opposite conclusions about the direction of lactate transport between neurons and astrocytes.

Also, to build a physiologically-plausible model, we need to have adequate and updated physiological knowledge. Therefore, we have to take into account new experiments and findings. These experiments can add to our knowledge about the parameters and underlying mechanisms. Finally, according to our review, even though artery lactate exists in other models, its contribution to brain energy metabolism is not studied explicitly.

3.3 Parameter Estimation

A challenging part of mathematical modeling is parameter estimation, especially when it comes to the brain. The parameters are determined by the experiments that have their limitations in capturing the exact dynamics and properties of the physiology. In any modeling problem, some of the parameters should be fixed using an optimization framework in steady state or using temporal data. Several techniques can be used depending on the complexity of the model's equations, number of desired parameters, and convexity of the equations.

3.3.1 Optimization

Mathematically, optimization means finding acceptable variables' values in order to minimize or maximize an objective function (cost function) of the desired variables, $f(\mathbf{x})$, and is formulated as;

$$min_{(\mathbf{x})}(f(\mathbf{x})), \mathbf{x} = (x_1, x_2, ..., x_n) \tag{16}$$

subject to:

$$\begin{aligned} g_i(\mathbf{x}) &\leq a_i, i = 1, 2, .., m \\ h_j(\mathbf{x}) &= b_j, j = 1, 2, .., p \\ lb &\leq x_k \leq ub, k = 1, 2, ..., n \end{aligned} \tag{17}$$

g_i and h_j are the i^{th} and j^{th} inequality and equality constraints on variables and similar to $f(\mathbf{x})$ can be either linear or non-linear while a_i and b_i are constant. Also each desired variable should lie in a plausible interval specified by its lower bound (lb) and upper bound (ub). Equations 16 and 17 together describe a *constrained optimization problem*. In some optimization problems, we have more than one objective function to optimize, which is called *multi-objective optimization*. Instead of solving a multi-objective optimization problem, we can build a scalar function from the weighted sum of squares of the cost functions [61].

Local vs. Global Optimum

Local optimum is an optimum point limited to its sufficiently close vicinity. A function can have more than one local minimum, but there is only one global minimum, which is also a local minimum. Figure 3.3a visualizes the difference between local and global minimum by an example in one dimension.

Based on this concept, functions can be categorized as convex (concave), in which there is only one global minimum (maximum), and non-convex. Mathematically, they are defined as functions with non-negative second derivatives. When the objective function is convex, The local and global optimum are the same. The problem becomes more complicated when it is non-convex. In this case, especially when there are multiple local optima, we should find the best local minimum as the global minimum. Figures 3.3b-3.3c are two examples of the functions with multiple local minima. These non-convex functions are harder to optimize because contrary to the convex problems, moving toward one direction does not guarantee convergence to the global minimum, which we are normally interested in.

3.3.2 Optimization Techniques

In this part, we briefly introduce some optimization techniques. the first two algorithms are gradient-based, and the others are heuristic methods.

Multi start

Multi Start (MS) is a gradient-based algorithm that exploits the Gauss-Newton approach. In this method, multiple sets of initial points are chosen in the parameter space. Then starting from the initial points and using a specific solver, it tries to approach the optimum point. At each step, MS updates the optimum parameter vector based on the cost function's gradient calculated for each parameter until it reaches the threshold [62, 63]. We can reduce the dependency of solutions on the initial guess by randomly choosing starting points, which helps the algorithm test different regions in the parameter space and not being trapped in the same local minimum.

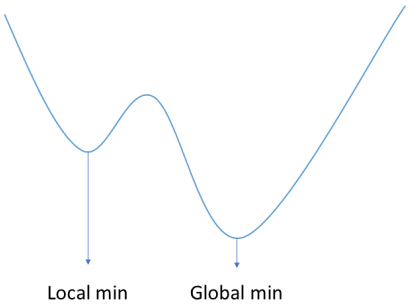

(a) Difference between local and global minimum

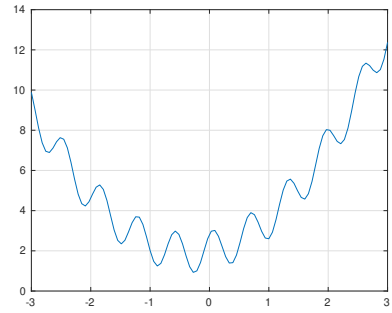

(b) $y = \frac{2x^3}{3} - 2xy - 5x + 2y^2 + 4y + 5$

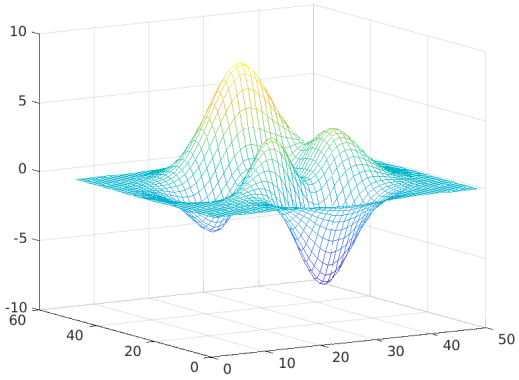

(c) Multiple translation and scaling of Gaussian distribution

Figure 3.3: Local vs. global minimum

Global Search

Global Search (GS) is similar to MS because they both do the local optimization for several starting points and then pick the best solution. The difference is that in GS, the starting points are generated by a scatter-search procedure. GS estimates basins of attraction (BOA) based on the user's provided initial point and then generates several sets of starting points based on the estimated BOA. Then it runs the local solver on each starting point [63].

Imperialist Competitive Algorithm

Imperialist Competitive Algorithm (ICA) is the genetic algorithm's sociopolitical counterpart, which utilizes the metaphor of imperialist competition. In this metaphor, countries are the parameter sets which we initially choose. An imperialist is a parameter set with minimum cost, and the

colonies in each empire have a higher cost compared to their associated imperialist [64].

First, several parameter sets are generated, and some are picked to be the imperialist and some as colonies. Then colonies are replaced toward imperialists, as shown in figure 3.4. There is also the probability of revolution in each iteration, meaning that newly generated ones may replace some sets in an empire. Finally, ICA converges to a single set of parameters with the minimum cost [65, 64]. The complete algorithm is depicted in Figure 3.3.2.

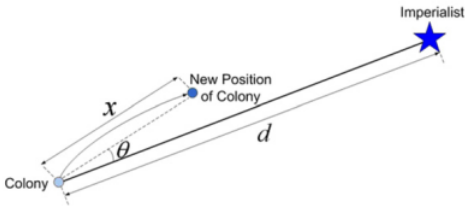

Figure 3.4: Assimilation in ICA

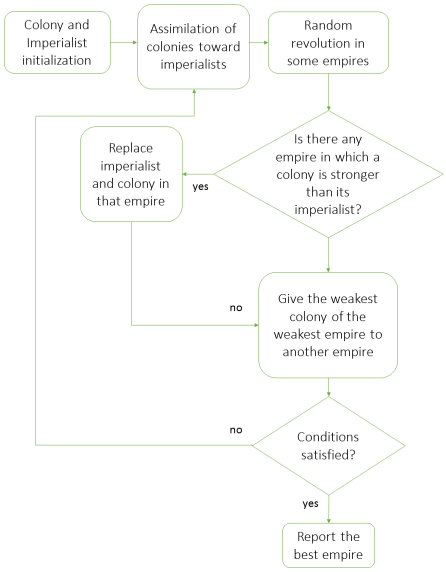

Figure 3.5: ICA algorithm

Pattern Search

Pattern Search (PS) falls under the algorithms that do a direct search for the optimization. In direct search, the algorithm does a grid search around a specific point to find the solution and does not need any orders of derivative. More specifically, PS chooses one point as the current point and calculates the objective function. Then it produces new points close to the current point by adding a vector to it to see if they can have a lower value compared to the current point's output or not. If so, then the current point will be updated to the point with lower function output, and if not, PS will start searching a closer vicinity of the current point. PS is useful for non-smooth objective functions [63].

Genetic Algorithm

Genetic algorithm (GA) is a heuristic method inspired by the theory of evolution. In this method, the space of parameters is encoded in the gene strings and then the populations of the possible solutions are created. These candidate solutions evolve, and in each step, the parameter sets with the lowest cost (fittest solutions) survive [61, 62].

Goal attainment method

The goal attainment method (GT) can be used for multi-objective optimization without using the sum of squares of the objectives. In multi-objective problems, sometimes there is a conflict between optimizing two functions simultaneously i.e., all objectives cannot be minimized at the same time [66]. GT is expressed as [63]:

$$minimize\ \gamma \tag{18}$$

Such that:

$$F_i(x) - w_i\gamma \leq F_i^*, i = 1, ..., m \tag{19}$$

F_i^* is the i^{th} objective. The term $w_i\gamma$ adds a flexibility to the problem. The weighting vector, w, enables the user to inject a relative trade-off between the objectives. For example, setting w equal to the initial goals indicates that the same percentage under- or overachievement of the goals, F^*, is

achieved [63]. One implementation of goal attainment that I used in Matlab is *fgoalattain* (FG).

Chapter 4

Proposed Lactate Model and Analysis

4.1 Introduction

In this chapter, we introduce the proposed lactate model with the equations and parameters. Then the preliminary results of optimization and resting state analysis are included. Finally, we tested the model's ability to simulate different scenarios.

4.2 Overview of the Model and Compartments

Our proposed model comprises four different compartments, namely pyramidal neuron, astrocyte, capillary, and extracellular space. The model is neutral concerning the direction of lactate transport, meaning that there is the possibility of both uptake and release of lactate for all the compartments. The model includes two primary sources of lactate: (1) local production inside the pyramidal cells and astrocytes, and (2) lactate from arteries, and can be consumed by the pyramidal cells and astrocytes. According to the current literature, access of neurons to the blood-brain barrier is restricted, and astrocytes' endfeet is mainly in contact with the capillaries. It is suggested that 90% of glucose metabolism taking place in the gray matter happens in the astrocytes [67, 68]. Therefore, in our model, we consider astrocytes as the only compartment in touch with the capillaries. Compared to other models of lactate, (1) we introduced new equations for the exchange of lactate between compartments and lactate production/consumption, (2) we analyzed the extent of lactate transport

rates in resting state as a result of choosing a different set of physiological parameters, and (3) we focused on analyzing the effect of arterial lactate changes on tissue lactate dynamics. The scale of the model is 1-gram brain tissue. Figure 4.1 is a schematic illustration of the proposed model

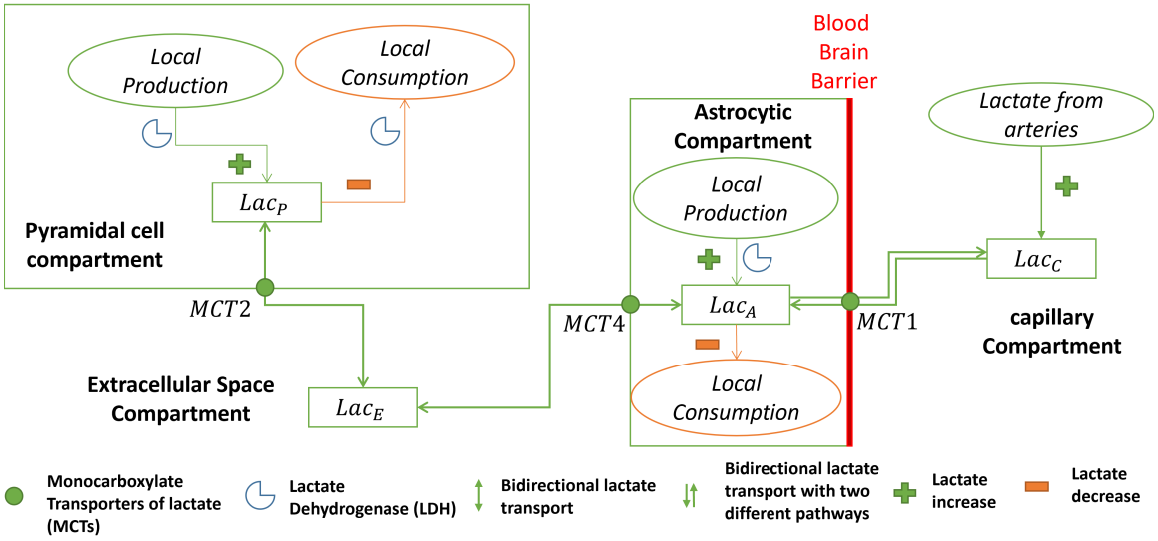

Figure 4.1: This figure is a schematic representation of the proposed lactate model. The astrocytic compartment works as a gate for exchanging lactate with the capillary, and this lactate uptake from the capillary increases during exercise or due to injection. MCTs carry lactate across the cell membrane and can be found in different isoforms, including MCT1, MCT2, and MCT4. The arrows show the pathways. LDH is the enzyme that catalyzes the reaction of lactate production and consumption.

In the following sections, we will introduce each compartment and its corresponding equations for lactate turnover. $\boldsymbol{Lac_X, X = P, E, A, C}$ are system's states (variables) and show lactate concentration inside pyramidal neuron, extracellular space, astrocyte, capillary, and artery, respectively. In the rest of this thesis, we refer to transport and production-consumption equations/parameters as MCT and LDH equations/parameters, respectively. To distinguish between system's states and parameters, we use bold notation for the states and normal notation for the parameters.

4.2.1 Pyramidal Neuron

As discussed in chapter 2, we only consider pyramidal neurons. In this model, there is the chance of release and uptake of lactate between pyramidal neurons and extracellular space through

a bidirectional pathway. We model this process by a simplified version of reversible Michaelis-Menten similar to an enzymatic reaction rate as described in [67]. The rate is given by:

$$V_{EP} = \frac{V^m_{E\to P}(\boldsymbol{Lac_E} - \boldsymbol{Lac_P})}{K^m_{E\to P} + \boldsymbol{Lac_E} + \boldsymbol{Lac_P}} \tag{20}$$

$V^m_{E\to P}$ is the maximal rate of transport between extracellular space and pyramidal cells, and $K^m_{E\to P}$

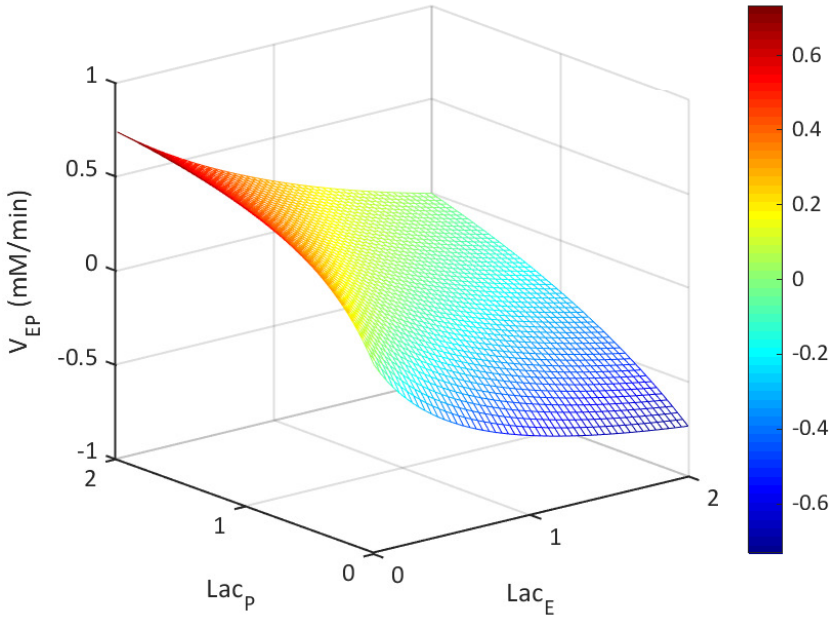

Figure 4.2: Reversible Michaelis-Menten model of V_{EP}

is its corresponding Michaelis constant. When $V_{EP} > 0$, it means that lactate is transported from extracellular space to the neuronal compartment and vice versa. The plot for equation 20 for certain range of Lac_P and Lac_E is visualized in Figure 4.2.

As mentioned in section 2.2.1 of chapter 2, lactate is produced from pyruvate in the last step of glycolysis, and the consumption of lactate happens in the opposite direction. We model this conversion by a double Michaelis-Menten equation [69]:

$$Prod_P = \frac{V_P^{prod} Pyr_P}{K_P^{prod} + Pyr_P}, Cons_P = \frac{V_P^{cons} \boldsymbol{Lac_P}}{K_P^{cons} + \boldsymbol{Lac_P}} \tag{21}$$

With V_P^{prod} and V_P^{cons} being the maximal rate and K_P^{prod} and K_P^{cons} being the Michaelis constant for the production and consumption, respectively. Pyr_P is the concentration of pyruvate in pyramidal neuron compartment. Combining both terms, we can represent the net lactate production as:

$$J_P = Prod_P - Cons_P \tag{22}$$

Parameter values for the equations 20, 21 are included in Table 4.1.

Table 4.1: Parameter values for equations 20 and 21[1]

Parameter	Unit	Value
$V_{E\to P}^m$	$mM.min^{-1}$	1
$K_{E\to P}^m$	mM	0.7
V_P^{prod}	$mM.min^{-1}$	0.5
K_P^{prod}	mM	0.0454
V_P^{cons}	$mM.min^{-1}$	3.2234
K_P^{cons}	mM	8.5

In the following when we refer to neurons, we mean pyramidal neurons.

4.2.2 Astrocyte

Based on the current literature, it is widely accepted that astrocytes play a critical role in the brain's metabolism, even though there exist debates about the mechanism of its contributions. So, we consider astrocytes as part of our model. Astrocytes exchange lactate with the capillaries and extracellular space and have a significant contribution to lactate production. We modeled their interactions with the extracellular space by the following equation similar to V_{EP} as follows:

$$V_{AE} = \frac{V_{A\to E}^m(\boldsymbol{Lac_A} - \boldsymbol{Lac_E})}{K_{A\to E}^m + \boldsymbol{Lac_A} + \boldsymbol{Lac_E}} \tag{23}$$

$V_{A\to E}^m$ is the maximal rate of transport between extracellular space and pyramidal cells, and $K_{A\to E}^m$ is the Michaelis constant. $V_{AE} > 0$ means that there is lactate release by the astrocyte compartment to the extracellular space and vice versa.

[1] Values for $V_{E\to P}^m$ and $K_{E\to P}^m$ are based on the experiments in [70, 71]. Parameter values for LDH equations are obtained after an optimization process explained in section 4.3.2.

For the lactate transport between astrocytes and capillaries, we considered a model of double Michaelis-Menten kinetics compared to the reversible model of V_{EP} and V_{AE}. Because in this case, we have two different pathways of release and uptake. This transport equation is written as:

$$V_{AC} = \frac{V^m_{A\to C}\boldsymbol{Lac_A}}{K^m_{A\to C} + \boldsymbol{Lac_A}}, V_{CA} = \frac{V^m_{C\to A}\boldsymbol{Lac_C}}{K^m_{C\to A} + \boldsymbol{Lac_C}} \tag{24}$$

$V^m_{A\to C}$ and $V^m_{C\to A}$ represent maximal rate of transport for the lactate transport from astrocyte to capillary and from capillary to the astrocyte, respectively. $K^m_{A\to C}$ and $K^m_{C\to A}$ are Michelis constants of the astrocyte-capillary transport rate. When $V_{AC} - V_{CA} > 0$, astrocyte releases lactate to the capillary while having $V_{AC} - V_{CA} < 0$ means that there is a net lactate uptake by the astrocyte.

Finally, two Michaelis-Menten equations are proposed (equation 25) to model lactate production and consumption. Even though astrocytes mainly produce lactate and their consumption is considerably lower, we still need the consumption term to regulate their production when there is an excess of lactate in the extracellular space or capillary.

$$Prod_A = \frac{V^{prod}_A Pyr_A}{K^{prod}_A + Pyr_A}, Cons_A = \frac{V^{cons}_A \boldsymbol{Lac_A}}{K^{cons}_A + \boldsymbol{Lac_A}} \tag{25}$$

With V^{prod}_A and V^{cons}_A as the maximal rate and K^{prod}_A and K^{cons}_A as the Michaelis constants for the production and consumption, respectively. Pyr_A is the concentration of pyruvate in pyramidal neuron. The net lactate production becomes:

$$J_A = Prod_A - Cons_A \tag{26}$$

Table 4.2 summarizes the parameter values for the equations 23-25.

4.2.3 Extracellular Space

Extracellular space is shared between astrocytes and pyramidal neurons. Its corresponding dynamics are modeled in the equations 20 and 23.

Table 4.2: Parameter values for equations 23-25[2]

Parameter	Unit	Value
$V^m_{A\to E}$	$mM.min^{-1}$	5
$K^m_{A\to E}$	mM	28
$V^m_{A\to C}$	$mM.min^{-1}$	0.1
$K^m_{A\to C}$	mM	1.9
$V^m_{C\to A}$	$mM.min^{-1}$	0.4
$K^m_{C\to A}$	mM	5.1
V^{prod}_A	$mM.min^{-1}$	0.6835
K^{prod}_A	mM	0.084
V^{cons}_A	$mM.min^{-1}$	0.08
K^{cons}_A	mM	1

4.2.4 Capillary

As mentioned above, capillaries interact with the astrocytes, and we mathematically represented this process in equation 24. The next part that contributes to the dynamics of the capillary compartment is CBF and artery lactate. This is represented by a model that is called the balloon model, and we took it from [51]. It is written as follows:

$$V_{cap} = \frac{2CBF(t)}{V_C}(Lac_J - \boldsymbol{Lac_C}) \tag{27}$$

In this equation, Lac_J is the artery lactate concentration, and V_C is the capillary volume. CBF is the cerebral blood flow. Parameter values for this equation are represented in Table 4.3.

Table 4.3: Parameter values for equation 27

Parameter	Unit	Value
V_C	-	0.0055
CBF_0	min^{-1}	0.012
Lac_J	$mM.min^{-1}$	0.88

Values of V_C and CBF_0 are derived from [51, 56] and value of Lac_J is based on [21]

Now that we have introduced modeled lactate kinetics in each compartment, we can write the

[2]Values of $V^m_{A\to E}$ and $K^m_{A\to E}$ are based on the experiments in [71, 72, 73]. For $V^m_{A\to C}$, $K^m_{A\to C}$, $V^m_{C\to A}$, and $K^m_{C\to A}$ values are derived from [74, 69]. Value of K^{prod}_A, V^{cons}_A, and K^{cons}_A are obtained from [75, 32] while V^{prod}_A is obtained after an optimization process explained in section 4.3.2.

summarized system of ODEs that describe behavior of this system as follows:

$$\begin{cases} F_1(t) = \frac{d\boldsymbol{Lac_P}}{dt} = \frac{V^m_{E\to P}\boldsymbol{Lac_E}-\boldsymbol{Lac_P}}{K^m_{E\to P}+\boldsymbol{Lac_E}+\boldsymbol{Lac_P}} + \frac{V^{prod}_P Pyr_P}{K^{prod}_P+Pyr_P} - \frac{V^{cons}_P \boldsymbol{Lac_P}}{K^{cons}_P+\boldsymbol{Lac_P}} \\ F_2(t) = \frac{d\boldsymbol{Lac_E}}{dt} = \frac{-1}{r_{EP}}\frac{V^m_{E\to P}(\boldsymbol{Lac_E}-\boldsymbol{Lac_P})}{K^m_{E\to P}+\boldsymbol{Lac_E}+\boldsymbol{Lac_P}} + \frac{1}{r_{AE}} + \frac{V^m_{A\to E}(\boldsymbol{Lac_A}-\boldsymbol{Lac_E})}{K^m_{A\to E}+\boldsymbol{Lac_A}+\boldsymbol{Lac_E}} \\ F_3(t) = \frac{d\boldsymbol{Lac_A}}{dt} = -\frac{V^m_{A\to E}\boldsymbol{Lac_A}-\boldsymbol{Lac_E}}{K^m_{A\to E}+\boldsymbol{Lac_A}+\boldsymbol{Lac_E}} + \frac{V^{prod}_A Pyr_A}{K^{cons}_A+Pyr_A} - \frac{V^{cons}_A \boldsymbol{Lac_A}}{K^{cons}_A+\boldsymbol{Lac_A}} \\ -\frac{V^m_{A\to C}\boldsymbol{Lac_A}}{K^m_{A\to C}+\boldsymbol{Lac_A}} + \frac{V^m_{C\to A}\boldsymbol{Lac_C}}{K^m_{C\to A}+\boldsymbol{Lac_C}} \\ F_4(t) = \frac{d\boldsymbol{Lac_C}}{dt} = \frac{2CBF(t)}{V_C}(Lac_J - \boldsymbol{Lac_C}) - \frac{1}{r_{AC}}(-\frac{V^m_{A\to C}\boldsymbol{Lac_A}}{K^m_{A\to C}+\boldsymbol{Lac_A}} + \frac{V^m_{C\to A}\boldsymbol{Lac_C}}{K^m_{C\to A}+\boldsymbol{Lac_C}}) \end{cases} \tag{28}$$

And the short form would become:

$$\begin{cases} F_1(t) = \frac{d\boldsymbol{Lac_P}}{dt} = V_{EP} + J_P \\ F_2(t) = \frac{d\boldsymbol{Lac_E}}{dt} = \frac{-1}{r_{EP}}V_{EP} + \frac{1}{r_{AE}}V_{AE} \\ F_3(t) = \frac{d\boldsymbol{Lac_A}}{dt} = -V_{AE} + J_A - V_{AC} + V_{CA} \\ F_4(t) = \frac{d\boldsymbol{Lac_C}}{dt} = V_{cap} - \frac{1}{r_{AC}}(-V_{AC} + V_{CA}) \end{cases} \tag{29}$$

$F_i(t), \quad i = 1, ..., 4$ in equations 28 and 29, corresponds to changes in lactate concentration in each compartment over time and is equal to the superposition of all transport and production/consumption rates.Except V_{cap}, which is a linear function of $\boldsymbol{Lac_C}$, other terms are non-linear functions. for instance V_{EP} is a non-linear function of $\boldsymbol{Lac_E}$ and $\boldsymbol{Lac_P}$. The coefficients r_{EP}, r_{AE}, and r_{AC} are called **volume fractions** and they will be introduced in more details in section 4.3.1.

4.3 Parameters

After defining the equations, **22 parameters** of the model should be determined. In this work, they are fixed based on the existing literature and experiments and optimization. In fact, for the MCT equations, we set the parameters to the more common values published in experimental literature for MCT parameters and some of the LDH parameters. However, for the other parameters in LDH equations, because the extent of the most parameters is large and the literature is poor on the subject, we defined an optimization problem constrained by the range of those parameters from the literature

and ran the optimization to have all the four ODEs equal to zero. In this case, there is not any change in the concentrations over time. Unknown parameters to be determined by optimization are as follows:

$$\Phi = \{V_P^{prod}, K_P^{prod}, V_P^{cons}, K_P^{cons}, V_A^{prod}\} \tag{30}$$

This set includes all the LDH parameters for the pyramidal neuron compartment and one out of four parameters of the astrocytic compartment. The optimization procedure will be discussed later in section 4.3.2 in more detail.

4.3.1 Volume Fractions

Looking back at F_2 and F_4 in equation 28and 29, we can see that exchange rate equations are multiplied by a few coefficients. These values correspond to the ratio of the volume occupied by each compartment in the brain tissue. In the computational models of brain metabolism, this is done to confine the space of the model to a specific well-mixed volume of the brain. This volume of the brain is usually chosen to be 1-gram brain tissue, and by having the density of the brain as $1.04 \frac{gr}{cm^3}$, this brain mass is equivalent to 0.96 cm^3. So, each equation will be scaled by a real-valued parameter as follows [57]:

$$V_r \frac{dL}{dt} = F(L), V_r = \frac{V_L}{V_0} \tag{31}$$

Where L is the metabolite concentration, V_r is the ratio of the modeled compartment volume to volume of 1-gram brain tissue. In another notation proposed in [50, 51], instead of scaling each ODE by the volume ratio factor, they only used the volume fraction scaling factor for the capillary and extracellular space compartment. In the next paragraph, we will explain that they are both equal.

Take V_{EP} as an example. Using the first notation, it would become $\frac{V_0}{V_P} V_{EP}$ in $F_1(t)$ and $-\frac{V_0}{V_E} V_{EP}$ in $F_2(t)$. On the other hand in equation 28, we have the coefficient $V^m_{E\to P}$ in V_{EP}. Based on the first notation, what we used in our model is $V^m_{E\to P} = \frac{V_0}{V_P} V^{m'}_{E\to P}$. So for $F_2(t)$, we need to multiply this coefficient by volume fractions. In fact it is multiplied by $\frac{V_P}{V_0}\frac{V_0}{V_E} = \frac{V_P}{V_E}$. In other words, $F_1(t)$ is taken as the reference, and then by this coefficient, we can return it to the correct scale. A similar logic is applied to other equations. We used the second formulation as it is widely utilized in the current literature of lactate models. Table 4.4 includes the values of volume fractions

used in the model and is based on [51].

Table 4.4: Volume fraction values

r_{EP}	r_{AE}	r_{AC}
0.444	0.8	0.022

4.3.2 Optimized Parameters

As mentioned before, due to the high variability in some LDH parameters in the literature, we only took the ranges of parameter values from previous experimental papers and optimized the resting state. We built an optimization problem to find the best values for them in neurons and astrocytes in order to minimize $F_i, i = 1, ..., 4$ in equation 28. Because we are doing the optimization in the resting state, the goal is to have $F_i = 0$. To solve this problem, we leveraged an auxiliary function to scalarize the objective function as shown in equation 32:

$$f_{obj} = \sum_{i=1}^{4} f_i^2$$
$$goal : f_{obj} = 0 \tag{32}$$

subject to:

$$LB \leq \Phi \leq UB \tag{33}$$

LB and UB are the lower and upper bound of the unknown parameters derived from the published experiments and is summarized in Table 4.5[3].

Table 4.5: Ranges of unknown LDH parameters in neurons and astrocytes

Parameter		V_P^{prod}		K_P^{prod}		V_P^{cons}		K_P^{cons}		V_A^{prod}	
lb	ub	0.5	60	0.03	0.07	0.24	28	0.3	8.5	0.5	70

In addition to these unknown LDH parameters, we have also four undetermined steady state concentrations. Therefore, we have **9 variables** to optimize. By concatenating Φ and these **4 steady**

[3]Ranges for V_P^{prod} and K_P^{prod} are taken from [76, 75], for V_P^{cons} and K_P^{cons} from [76, 75, 32], and for V_A^{prod} from [75],

states, our new set of unknown variables would become:

$$\Phi' = \{\Phi, \boldsymbol{Lac_P^{SS}}, \boldsymbol{Lac_E^{SS}}, \boldsymbol{Lac_A^{SS}}, \boldsymbol{Lac_C^{SS}}\} \tag{34}$$

with the ranges specified in Table 4.6. These ranges are based on typical values in the published models.

Table 4.6: Ranges of unknown steady states

Parameter		$\boldsymbol{Lac_P^{SS}}$		$\boldsymbol{Lac_E^{SS}}$		$\boldsymbol{Lac_A^{SS}}$		$\boldsymbol{Lac_C^{SS}}$	
lb	ub	0.2	5	0.44	0.88	0.8	1.2	0.8	1.2

Since our optimization problem is a high dimensional and non-linear problem, it will have multiple local minima, and the algorithm might trap in one of them. In order to prevent this, we do the following:

(1) running the optimization algorithm for several times to obtain as many solutions as we can,

(2) when the algorithm needs initialization of the unknown parameters, we randomly choose it from the range specified for them. So in each iteration of the algorithm, a new set of parameters is randomly chosen from the space of parameter values.

This will add to the diversity of solutions found in the optimization. Considering all these points, we might still have solutions that are not close to zero and will make the system drift from a steady state. In order to avoid this, we set a threshold and discard the parameter sets that result in the objective function to values higher than the threshold. The whole process is summarized in Figure 4.3.

4.3.3 Comparison of Optimization Algorithms

After defining the optimization problem, we ran each algorithm 2000 times to better understand their convergence behavior. We compare the behavior of the following algorithms: *genetic algorithm (GA), pattern search (PS), global search (GS), multi start (MS), imperialist competitive algorithm (ICA), and fgoalattain (FG)*. Figure 4.4 is attached in order to compare the algorithms in terms of finding the global minimum. It shows the best cost achieved during these 2000 simulations

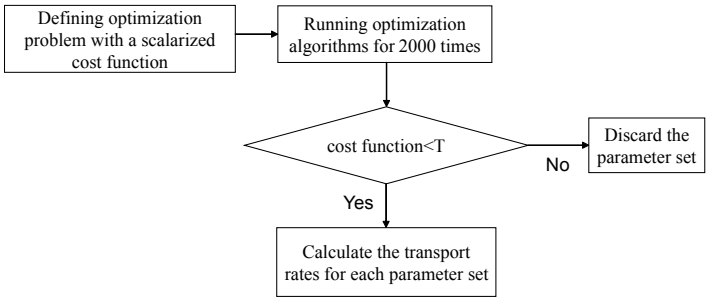

Figure 4.3: Procedure to optimize and analyze the model's resting parameters. T is a certain threshold which is set to 10^{-15}

of each algorithm. For all the algorithms except FG, the objective function is the scalarized one defined in equation 32. Because FG does a multi-objective, its objective function is a 4-by-1 vector, and it returns four values for the objective functions. So, the sum of squares of all returned objective function values is calculated to make its results comparable to other methods.

According to figure 4.4, in terms of reaching the minimum, FG, ICA, MS, and GS outperform GA and PS and converge to almost zero. Table 4.7 is also added in order to see the results in more detail. It includes the mean and the best cost of each method and also the average time it takes for the technique to do one iteration. As can be seen, ICA was able to return the lowest value, and in the next place, FG returns the most optimum objective value. MS and GS are similar in terms of the objective function value, but GS is a bit faster. According to this table, the fastest algorithm is FG and GA takes more time than the other methods to converge.

Another aspect of the solutions to discuss is their variations. As observable from the results, GA and PS show a higher difference between average and best cost, while this happens less in MS, GS, and ICA.

Table 4.7: Cost and time consumption of the algorithms

	GA	PS	GS	MS	ICA	FG
Mean cost	0.0156	0.0054	5.80e-7	3.22e-7	2.00e-12	2.73e-7
Best cost	3.18e-7	6.81e-7	6.28e-8	3.98e-8	1.55e-17	2.08e-14
Timing (S)	25.90	0.44	7.38	12.33	8.50	0.02

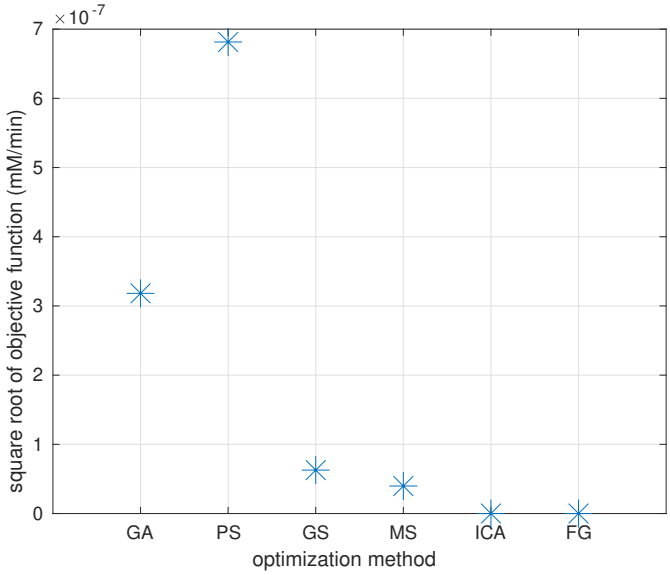

Figure 4.4: Comparison of different optimization algorithms in terms of value of objective function.

Based on the results in this section, we decided to use ICA as the optimization algorithm. However, it does not mean that using FG will affect the consequent results. In the next section, we analyze the general behavior of the system based on the obtained parameters in the optimization iterations.

4.4 Resting State Results

According to the optimization procedure explained in section 4.3.2 and Figure 4.3, we ran the optimization for 2000 iterations. Then 496 parameter sets out of all the obtained parameter sets were chosen conditional upon the minimization level. Each chosen parameter set results in the system's states remaining steady and their time derivative becoming zero. Figure 4.5 shows the distribution of the parameters and resting state concentrations using these parameters. Then, these are used to calculate intermediate variables such as lactate exchange rates between compartments and the differences between lactate production and consumption in the neuronal and astrocytic compartment. They are visualized in Figure 4.6. Finally, Figure 4.7 is included to specifically compare $\boldsymbol{Lac_P^{SS}}$ and $\boldsymbol{Lac_A^{SS}}$.

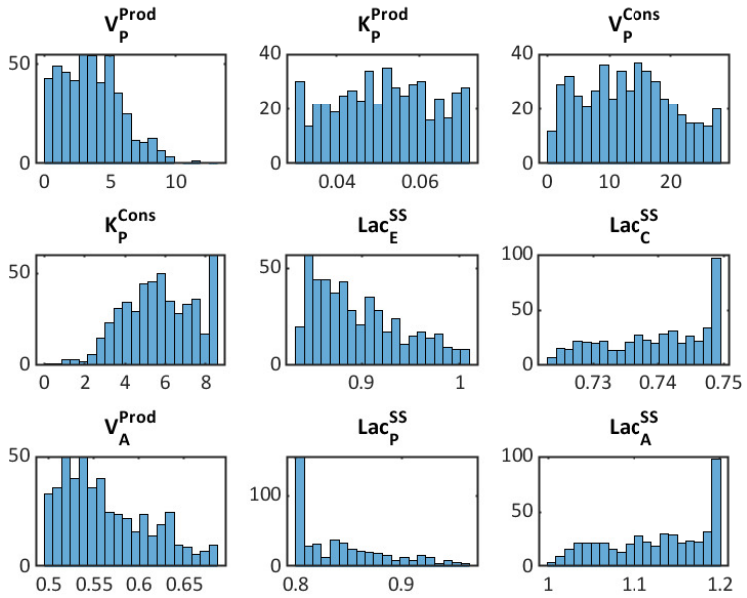

Figure 4.5: Distribution of obtained parameters in resting state optimization

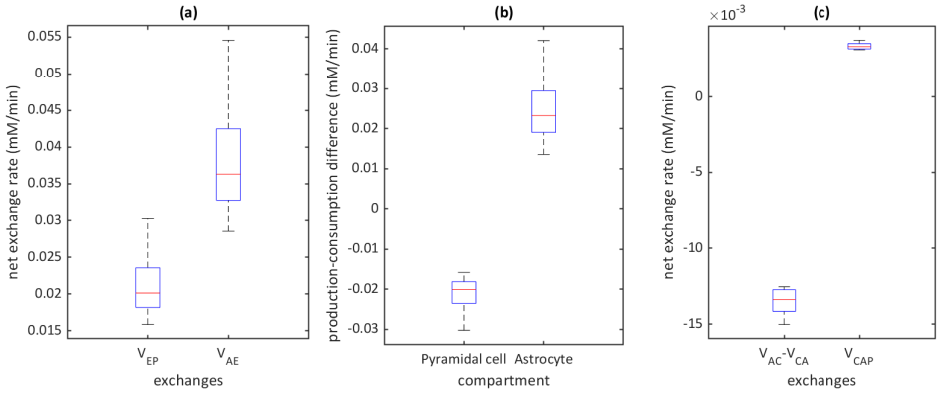

Figure 4.6: Distribution of calculated intermediary variables using 496 parameters obtained from optimization in resting state.

4.4.1 Discussion

According to Figure 4.5, obtained parameters are distributed over the specified range, and except for the resting concentrations, the optimization finds diverse sets of solutions. As can be seen from Figure 4.6, in our model in resting state, ANLS exists. Specifically, with V_{EP} being distributed on the positive side, neurons uptake lactate for the simulated physiological parameter sets. Also,

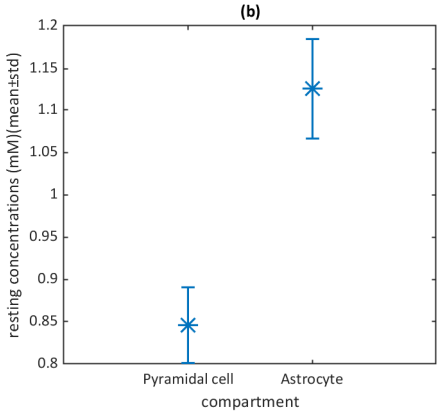

Figure 4.7: mean±std of Lac_P^{SS} and Lac_A^{SS} for the 496 parameter sets

we have positive values for V_{AE}, meaning that, on average, the astrocyte compartment releases lactate to the extracellular compartment. Consequently, we can say that in our model, in resting, we have ANLS to be functional in resting state. By having $J_P < 0$, neurons are, on average, lactate consumers. These observations are in accordance with the experiments in [2, 35, 34].

We also observed net lactate production inside astrocytes compatible with the physiological literature showing astrocytes to be more glycolytic [34]. For the astrocyte-capillary interface, we observe a negative quantity for the $V_{AC} - V_{CA}$ meaning that there is a net lactate uptake by the astrocyte compartment. This uptake is smaller compared to V_{EP} and V_{AE}. This observation is consistent with some of the values of resting lactate exchange rates between blood and the brain reviewed in [21]. However, there are values in this review showing the opposite direction, i.e. lactate is released to the blood from the brain in resting conditions.

Finally, According to Figure 4.7, we see a significant difference between the resting concentrations of neurons and astrocytes. Resting concentration of lactate in the astrocytes is higher and this is in agreement with the results of many experiments such as [35, 34].

4.4.2 Effect of Changing Pyr_P, Pyr_A

In our proposed model, as we did not explicitly model dynamics of pyruvate, we fixed its concentration in the neuron and astrocyte compartments. For resting state, based on the literature, we choose $Pyr_{P,0}$ to be $1/18$ of Lac_P^{SS} and $Pyr_{A,0}$ to be $1/100$ of Lac_A^{SS} [77, 50, 51]. To assess the

effect of fixing different values of Pyr_P and Pyr_A of the equations 21 and 25, on the resting state behavior of the model, we tried a wide range of values. In this process, we assigned different values to pyruvate concentration and ran the ODE solver for a long time to converge to the new resting state concentrations. In these simulations, we tested the concentrations in the following range:

$$0.05Pyr_{X,0} \leq Pyr_X \leq 10Pyr_{X,0}, \quad X = A, P$$

As a result, a grid of different model behaviors based on various pyruvate concentrations is obtained. In this grid, we see four different regions corresponding to four different behaviors as depicted in Figure 4.8. To summarize the figure, V_{AE} is not included because in resting its sign is the same as V_{EP} (refer to $F_2(t)$ in equation 28).

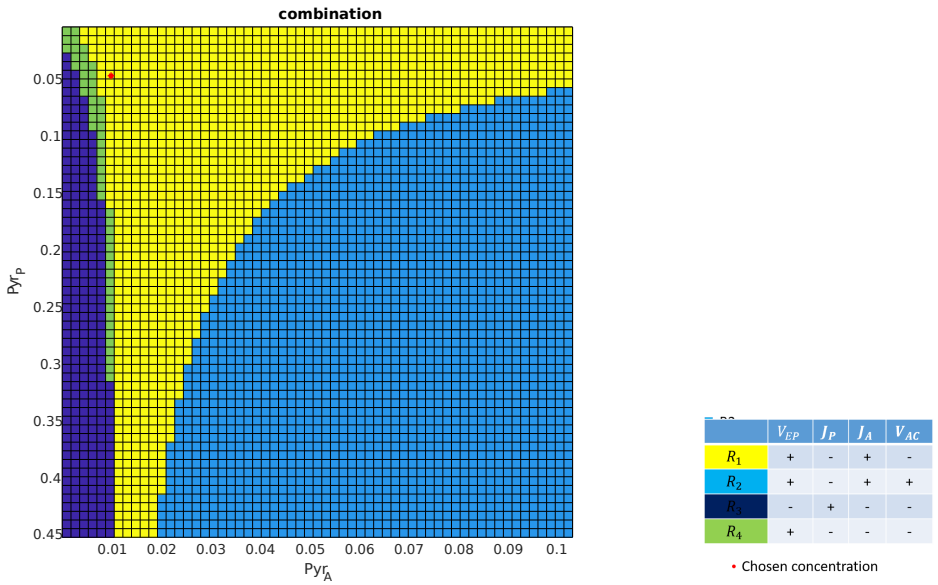

Figure 4.8: Grids of Pyr_P and Pyr_A that categorizes system's behaviour in resting state into four different regions shown by different colors.

R_1 is a region representing usual characteristics that we already observe in the model. In this region, lactate is released from astrocyte to the extracellular space and neurons uptake and consume lactate. By increasing Pyr_A, the system switches to region R_2 where it keeps ANLS but with only astrocytes' production as source of lactate. In this region, part of astrocyte's lactate is released to the capillaries. For the same value of Pyr_A, this effect is reinforced by increasing Pyr_P. By decreasing pyruvate concentration inside astrocytes to low values, the model's response moves to region R_3. In R_3, we see a switch from ANLS to NALS, where neurons become lactate producers and astrocytes

switch to a consumer which is not a typical behaviour. In some rare cases region R_4 is seen where the model enters a situation that both neurons and astrocytes become lactate consumers. R_3 and R_4 are regions with atypical behavior where astrocyte compartment consumes lactate. This behavior is due to considering very low values for Pyr_A that can be beyond the physiological range. These two regions might also resemble a situation where astrocyte function is impaired in production of pyruvate from glucose or less glucose uptake. In the next sections we will analyze the behavior of the model where pyruvate concentration changes in a short period of time.

4.5 Temporal Dynamics Simulations

After analyzing the model's behavior in resting state, we can explore its response over time in a limited period of perturbation. The built-in solvers of the MATLAB, including *ODE45* and *ODE15s*, were used to simulate the model in the dynamic mode, the

We consider the following scenarios to examine:

(1) increased lactate production in the neurons and the possibility of a switch to NALS,

(2) increased lactate production in the astrocytes,

(3) increased energy demand in the neurons and increased artery lactate

The simulations are done to evaluate the validity of the model's response and to understand the extent of observations we can have from the proposed model. We define some input functions for a few model parameters that can change over time for these simulations. They are introduced in the next section.

4.5.1 Time Dependant Parameters

In our lactate model, some parameters can vary over time. For instance, when the neurons are activated, blood flow increases to support elevated activity. We also fixed the pyruvate concentration, which does not hold in all the cases and can change. In the following, we will introduce the functions and their parameters used as inputs to run the dynamical simulations.

CBF

We consider a double exponential model for CBF similar to [60]:

$$CBF(t) = \begin{cases} CBF_0 + CBF_1(exp((-t+t_1)/2) - exp((-t+t_1)/0.1)), & t_1 \leq t \leq t_{end} \\ CBF_0(1 + (CBF(t_{end}) - CBF_0)exp(t_{end} - t/20)), & t > t_{end} \\ CBF_0 \quad t_{end} << t < t_1 \end{cases} \tag{35}$$

This curve is shown in Figure 4.9a.

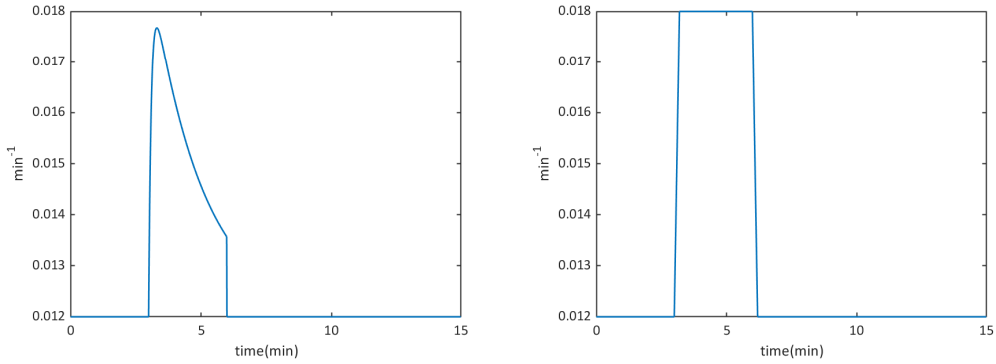

(a) (b)

Figure 4.9: Chosen functions for time-dependant parameters. (a) Trapezoid function used for Pyr_P, Pyr_A, and Lac_J, (b) double exponential function used to model CBF over time.

Neuronal and Astrocytic Pyruvate (Pyr_P, Pyr_A)

To test the effects of perturbing pyruvate concentration on lactate dynamics, we simulate multiple scenarios which resembles different physiological conditions. This variability include either increase or decrease over time. The general model we use for them is a trapezoid function with

linear slope:

$$Pyr_X(t) = \begin{cases} Pyr_{X,0}, \quad 0 < t < t_1 \quad and \quad t_{end} < t < L \\ Pyr_{X,0} + (Pyr_{X,1} - Pyr_{X,0})(t - t_1)/t_d, \quad t_1 < t < t_1 + t_d \\ Pyr_{X,1}, \quad t_1 + t_d < t < t_{end} \\ Pyr_{X,1} + (Pyr_{X,1} - Pyr_{X,0})(t - t_{end})/t_d, \quad t_{end} < t < t_{end} + t_d; \end{cases} \tag{36}$$

where $Pyr_{X,1}$ is the elevated value of pyruvate concentration which we will determine according to the simulation scenario.

Artery Lactate (Lac_J)

As mentioned before, artery lactate varies due to injection or physical exercise. So by changing its corresponding parameter in the model (Lac_J) over time we can asses its effect on brain tissue. Similar to pyruvate, we consider a trapezoid function for artery lactate as shown in Figure 4.9b. Temporal parameters are summarized in Table 4.8.

Table 4.8: Parameter values of dynamical simulations. All values are in minutes.

t_1	t_d	t_{end}	L	dt
3	0.2	6	30	0.005

For the following simulations we use the parameter values mentioned in Tables 4.1-4.4. As mentioned before, some of these parameters are set by using experiments in the literature. Others are determined based on the optimization procedure explained in section 4.3.2. As we want to use one parameter set for the rest of our analysis, we chose the one with the lowest objective function value. Values of these parameters can be seen in Tables 4.1-4.2. The resting concentrations that arise as a result of this combination of parameters are included in Table 4.9.

Table 4.9: Resting state lactate concentrations in mM for the chosen parameter set

Lac_P^{SS}	Lac_E^{SS}	Lac_A^{SS}	Lac_C^{SS}
0.8121	0.8522	1.0349	0.7273

We also tested the effect of disturbances on the resting states. In fact, we started the ODE solver

at different initial points and checked their convergence to the chosen resting states as shown in Figure 4.10.

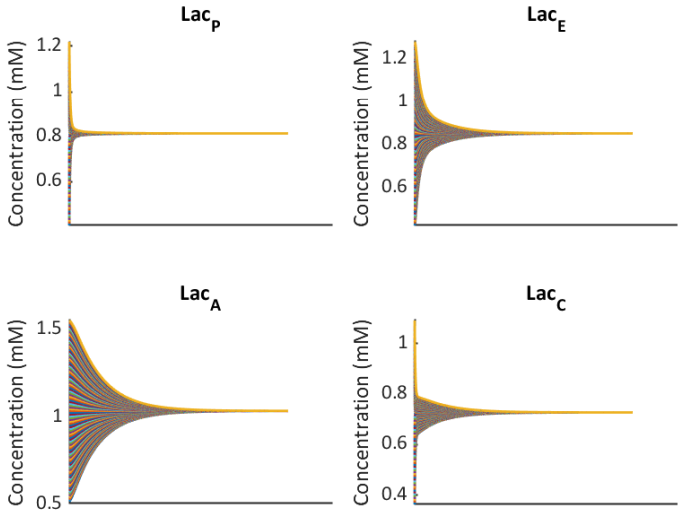

Figure 4.10: Convergence of steady states to the initial chosen resting states by 50% perturbation

4.5.2 Scenario I: Elevated Pyr_P

For the first scenario to simulate, we increased pyruvate concentration inside neurons to 5 different values for a 3-minute interval as indicated in Figure 4.11a. This scenario resembles a situation where conversion of glucose to pyruvate increases due to activation and we have more glycolysis activity. We also increased CBF to 1.5 times its baseline value during activation.

A trivial result of this set of inputs is that concentration of lactate in each compartment increases. According to the blue curves in Figure 4.11b (corresponding to no pyruvate change), CBF causes only a slight increase in the concentrations. Additionally, we can see that lactate increase inside neurons is higher than astrocytes because the latter is directly affected by CBF increase. When pyruvate is elevated, we see more increases in the concentrations.

To have a closer look at what happens to the intermediary variables, Figures 4.11c and 4.11d are included. Due to the escalated pyruvate concentration, lactate production in neurons grows, and after a certain threshold, it becomes positive and makes the neurons a net lactate producer. Kinetics

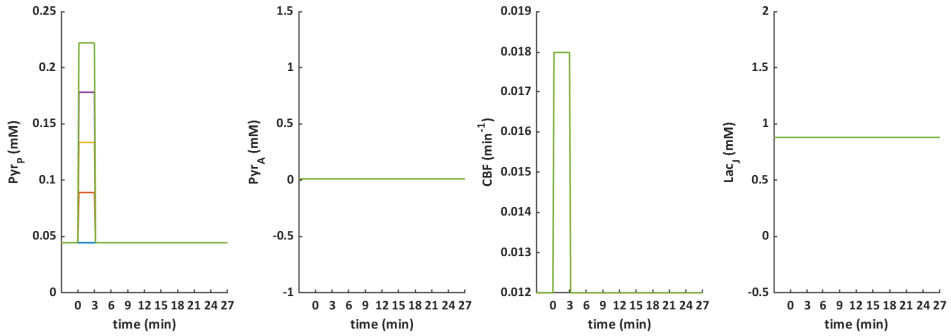

(a)

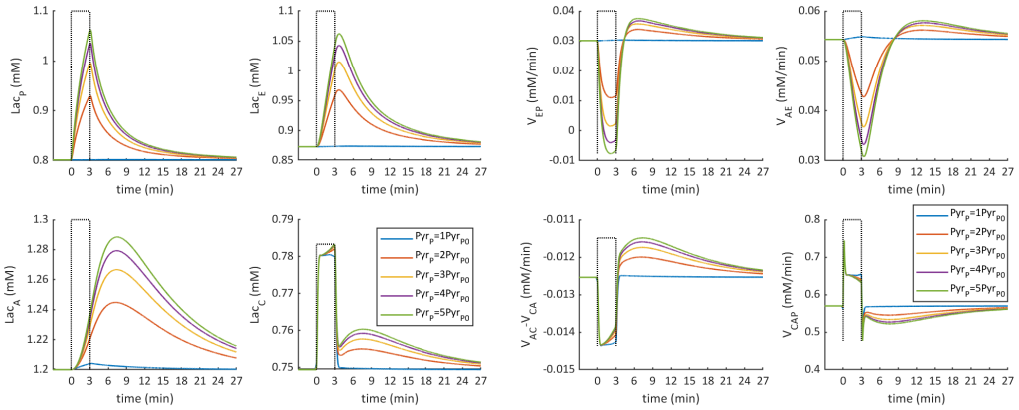

(b) (c)

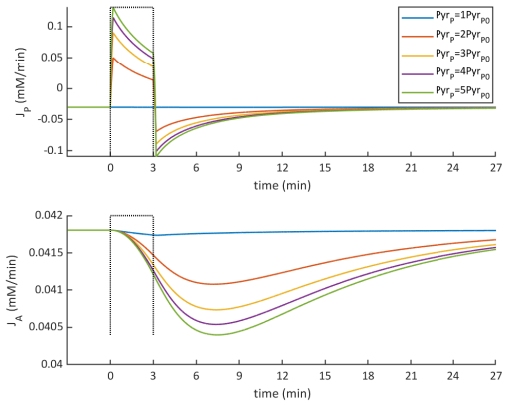

(d)

Figure 4.11: Simulation results of elevated Pyr_P scenario. Dashed lines represent the activation period and different colors correspond to different levels of Pyr_P. (a) Shows the inputs of the model. There are only changes in Pyr_P and CBF. (b) Includes the dynamics of lactate concentration inside all compartments, (c) contains the temporal evolution of lactate exchange rates, and (d) visualizes the LDH curves for neuronal and astrocytic compartment.

of V_{AE} show that by increasing Pyr_P, lactate release by astrocytes decreases but does not become negative, which means that there is still lactate release by the astrocytes. A reason might be the time interval of simulations because according to F_2 in equation 28, V_{AE} follows V_{EP} in reaching the equilibrium. If we extend the time of activation, V_{AE} reaches negative values meaning that astrocyte uptakes lactate from the extracellular space.

Even though there is a sharp increase in the lactate production in neurons, but it settles down as the system passes the onset of activation (Figure 4.11d). Another observation from the LDH curves is that convergence of J_A is slower compared to other rates. We can also see a tendency toward saturation when the pyruvate concentration reaches its maximum values, which is expected because of the nature of Michaelis-Menten equations used in the model.

4.5.3 Scenario II: Elevated Pyr_A

For the next paradigm, we increased astrocyte pyruvate gradually until 5 times its initial value (Figure 4.12a). This case represents increased glycolysis in the astrocytes that in the first place contributes to the lactate production inside astrocytes. Similar to section 4.5.2, CBF is stimulated to reach 1.5 times its resting value. Consequently, lactate concentration inside all compartments increases as shown in 4.12b. This time, we see a considerably larger rise in the Lac_A compared to Lac_P.

Based on the results in Figure 4.12c, transport of lactate from extracellular space to the neuronal compartment grows as a function of Pyr_A and emphasizes the role of ANLS. Two different phases for $(V_{AC} - V_{CA})$ can be considered. First, due to the initial increase in CBF and consequently in V_{CAP}, $(V_{AC} - V_{CA})$ experiences an initial decrease which remains stable until the end of the paradigm when there is no rise in Pyr_A (blue curve). Nevertheless, in other cases, it will change to a rise in $(V_{AC} - V_{CA})$ which leads us to the second phase, in which transport of lactate is retrieved and even rises to the values higher than its basal concentration. Finally, because we stabilized neuronal pyruvate during activation, we will see more lactate consumption in them and an increase in astrocytes, as visualized in Figure 4.12d.

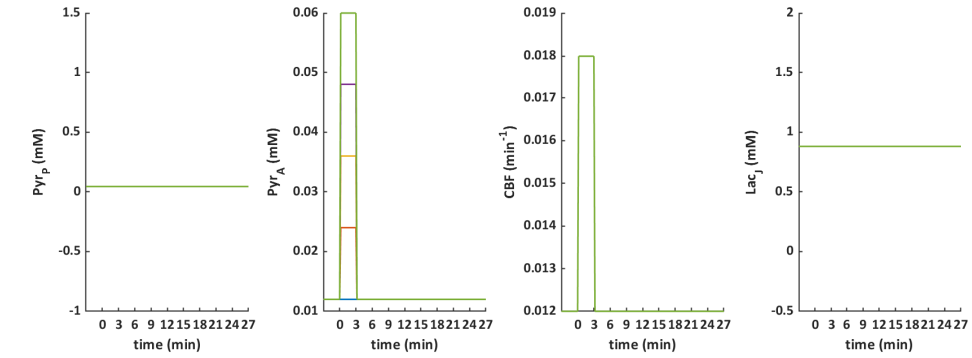

(a)

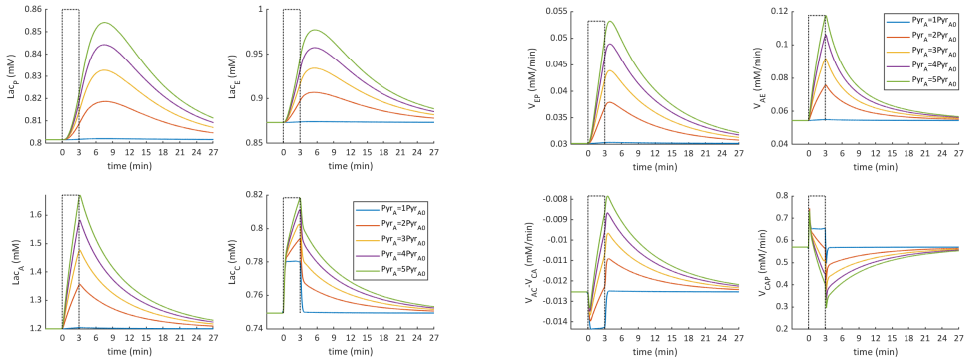

(b) (c)

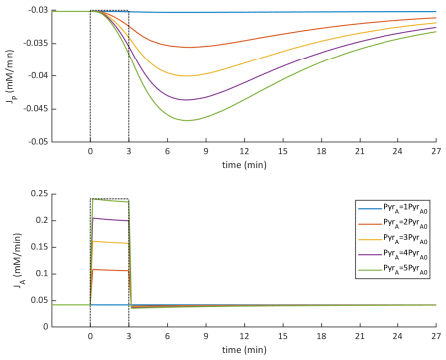

(d)

Figure 4.12: Simulation results of elevated Pyr_A scenario. Dashed lines represent the activation period and different colors correspond to different levels of Pyr_A. (a) Shows the inputs of the model. There are only changes in Pyr_A and CBF. (b) Includes the dynamics of lactate concentration inside all compartments, (c) contains the temporal evolution of lactate exchange rates, and (d) visualizes the LDH curves for neuronal and astrocytic compartment.

4.5.4 Scenario III: Increased Energy Demand

In the third scenario, we first analyze the effect of artery lactate on energy demand in neurons and then compare that to the impact of Pyr_A. The inputs are shown in Figure 4.13a. We gradually increased artery lactate to 8.8 mM while keeping a 2% drop in Pyr_P. The former can happen due to lactate injection or physical exercise. The latter indicates less pyruvate production from glucose and energetic needs in neurons due to activation. An increase in Lac_J is considered variable depending on the injection level, exercise intensity, and personal traits, so we simulated different concentrations to capture all possible situations.

In the first place, we can examine neuron's response to the decrease in Pyr_P without any change in Lac_J as shown in blue curves in Figures 4.13b-4.13d. In this case, lactate is less produced, and lactate transport cannot compensate for it. So, we see a slight but constant decrease in Lac_P as depicted in Figure 4.13b. The increased transport of lactate can be seen in the rise of V_{EP} and the decay in Lac_E curve.

Next, by raising the value of Lac_J, we observe that even though the initial dip in Lac_P still exists, the delivered lactate from arteries and through the ANLS mechanism compensated the initial dip. This phenomenon can be seen by looking at the increase in the transport of lactate from capillary to the astrocyte and then to the neuron via extracellular space as shown in Figure 4.13c. Finally, we see that lactate consumption grows and results in pyruvate production, which then can be used in energy production.

To compare the impact of lactate production and artery lactate on the initial dip, we constructed a set of inputs as shown in Figure 4.14a. Astrocyte pyruvate is swept from its baseline to 5 times more while Lac_J changes from its resting concentration to 8.8 mM. Pyr_P is kept at 98% of its basal concentration.

According to Figure 4.14b, a trivial conclusion is that the higher the artery lactate, the less the initial dip is. The initial dip decreases exponentially with the increased artery lactate. Nevertheless, this effect saturates by increasing astrocyte pyruvate. We observe that the initial dip drops dramatically by the first increase in Pyr_P, but it does not vary too much after that. Notably, our model suggests that lactate production inside astrocytes can diminish the effect of lactate coming from

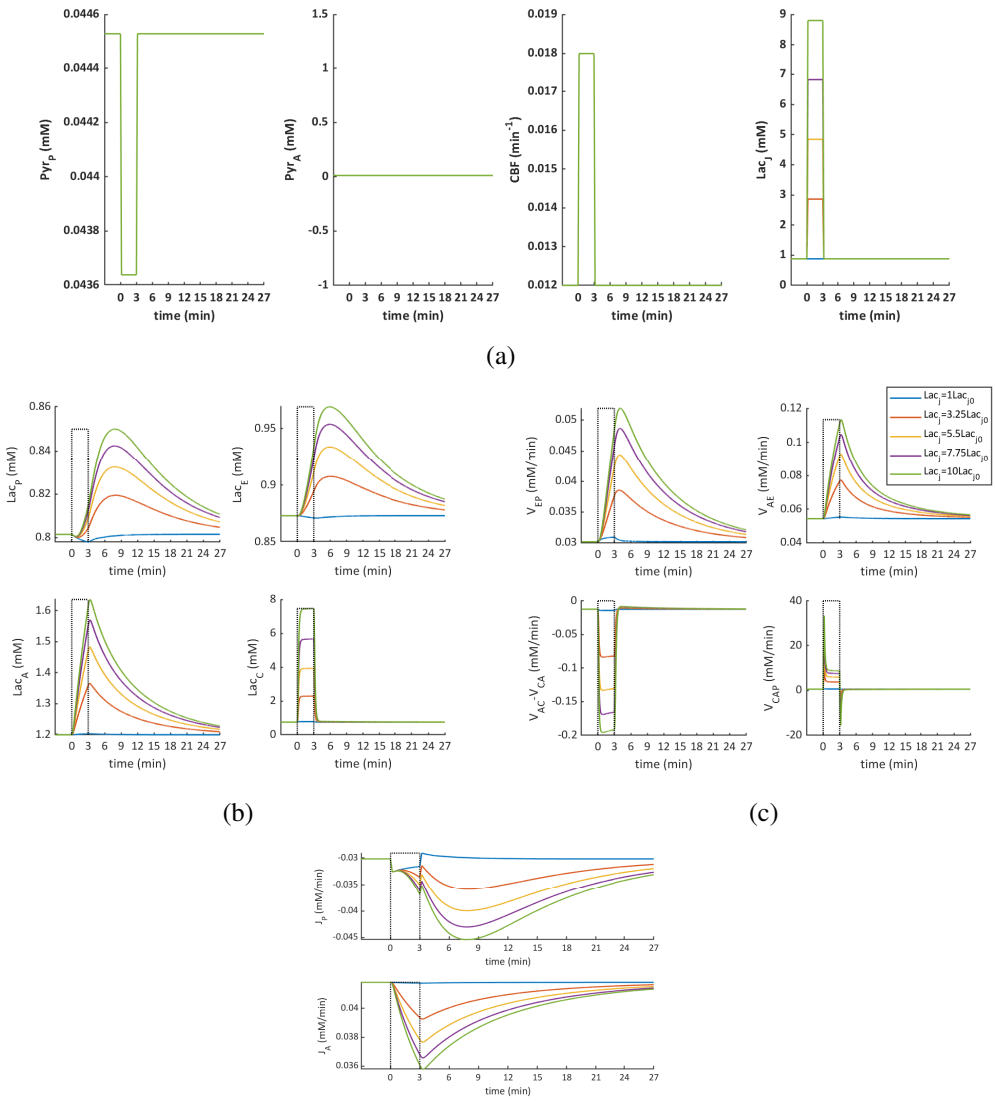

Figure 4.13: Simulation results of increased energy demand scenario. Dashed lines represent the activation period and different colors correspond to different levels of Lac_J. (a) Shows the inputs of the model. (b) Includes the dynamics of lactate concentration inside all compartments, (c) contains the temporal evolution of lactate exchange rates, and (d) visualizes the LDH curves for neuronal and astrocytic compartment.

arteries.

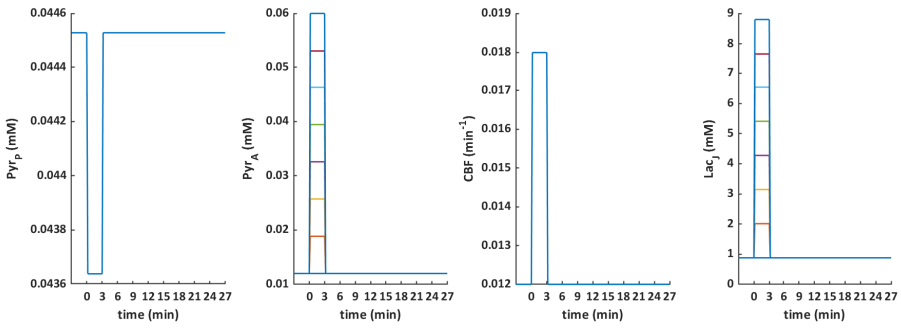

(a)

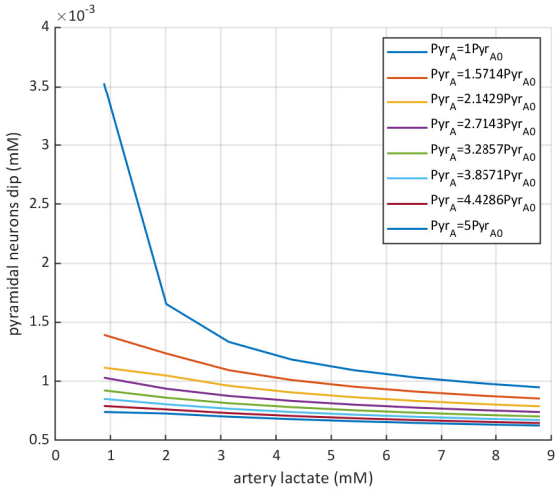

(b)

Figure 4.14: (a) Shows how the time dependant parameters are organized in the paradigm of increased energy demand, and (b) is a curve depicting the effect of Pyr_A and Lac_J in reducing the initial dip seen in Lac_P in increased energy demand scenario. Different colors are associated with different levels of Pyr_A.

Chapter 5

Conclusion and Future work

5.1 Conclusion

In this thesis, we proposed a novel mathematical model for brain lactate exchanges. We modeled lactate dynamics in pyramidal neuron, astrocyte, extracellular space, and capillary compartments using double Michaelis-Menten and reversible enzyme kinetics. We considered both transport and production/consumption of lactate. For the model parameters, we leveraged experiments in the literature to either fix or determine the physiological ranges of the parameter values. Using an optimization in resting state, we obtained acceptable parameter sets and analyzed possible behaviors of the model with these parameters.

In the next step, we tested the robustness of the model's responses when perturbing a few parameters. For this aim, we first swept the values for pyruvate concentration inside neuron and astrocyte. We qualified the system's behavior in resting i.e., when the system has enough time to converge to its new resting state. Second, we examined the robustness when there are temporary perturbations that resemble physiological scenarios. These scenarios include: (1) escalating Pyr_P as an indicator of increased glycolysis in neuron, (2) elevating Pyr_A as a representative of increased glycolysis in astrocyte, and (3) increased Lac_J, as a result of lactate injection or physical exercise.

In general, our results show that even though the dominant behavior of the model is ANLS, the model is also capable of showing the opposite direction of lactate transport from neurons to astrocytes (NALS). In particular, in resting conditions, the model shows net lactate uptake by neurons.

This lactate comes from the lactate production inside astrocytes and the blood supply to the brain through the artery. This behavior is compatible with current literature [2, 78, 42]. We also found a net lactate uptake by the astrocytes from capillaries. Referring to [21], we see that even though a net release is seen in most experiments, in some cases, uptake can take place. We can also see that the values of arterio-venous difference are close to zero as in our model.

On the other hand, in some situations, there is the possibility of a switch to NALS where neurons release lactate and astrocytes uptake this excess lactate. This happens when glycolysis in the astrocytes decreases, which can be due to the lower supply of glucose. This switch is reported in the literature [33, 39]. It can also be a pathological behavior of the astrocyte. Finally, based on our results we showed that in situations with higher energy demand in neurons, artery lactate can compensate for the initial drop in lactate concentration in neurons with a delay. In this case, lactate is behavior is achieved with the lactate shuttling property of astrocytes. This suggests that lactate increase due to injection or physical exercise can affect neurons and their metabolism, compatible with the experimental studies reviewed in [21].

5.2 Future Work

This work can be extended in terms of modeling and analysis. Here are some research directions:

- This model can be extended to include glucose and pyruvate metabolism to build a complete metabolic model. In this case, instead of fixing time variations of pyruvate as an indicator of glycolysis, its dynamics can be determined by the kinetics of glucose and we can directly modify glucose uptake as the main energy substrate of the brain. The next step would be to integrate the metabolic and electrophysiological models to examine the connection between metabolism and brain activity. This link is physiologically embedded in the synchronization of glutamate uptake, and lactate release by the astrocytes and also CBF [18, 34]. These models can also extend to study specific brain networks and include variations in different brain nodes' metabolism.

- We can rearrange the model in order to embed other features of transporters such as transacceleration. Transacceleration is a property of MCTs that can cause release of a substrate (e.g. lactate) when another monocarboxylate molecule (e.g., pyruvate) is present in the extracellular [79]. By modeling pyruvate and considering the same transporters for that, this feature can be investigated.

- One of the challenges in modeling brain metabolism is having access to the real temporal dynamics of metabolites to validate the model's results. A technique which is used in recent years to measure lactate dynamics is using genetically-encoded Forster Resonance Energy Transfer (FRET)-based lactate sensor [80]. The problem is that the sensor's output is not quantitatively comparable with the model because its values are not concentrations. An in-vivo calibration is needed to convert it to acceptable units but this calibration needs new experimental data. Having that, by doing an optimization in the dynamical state, one can fit the model's results to the experimental data and compare the outputs to real data.

- Sensitivity analysis can be done to quantify the impact of perturbing each parameter on the model's temporal outputs [81]. Additionally, probabilistic methods such as Markov chain Monte Carlo can be used in order to take the noise and uncertainty over the parameters and states into account.

Appendix A

Glycolysis Pathways

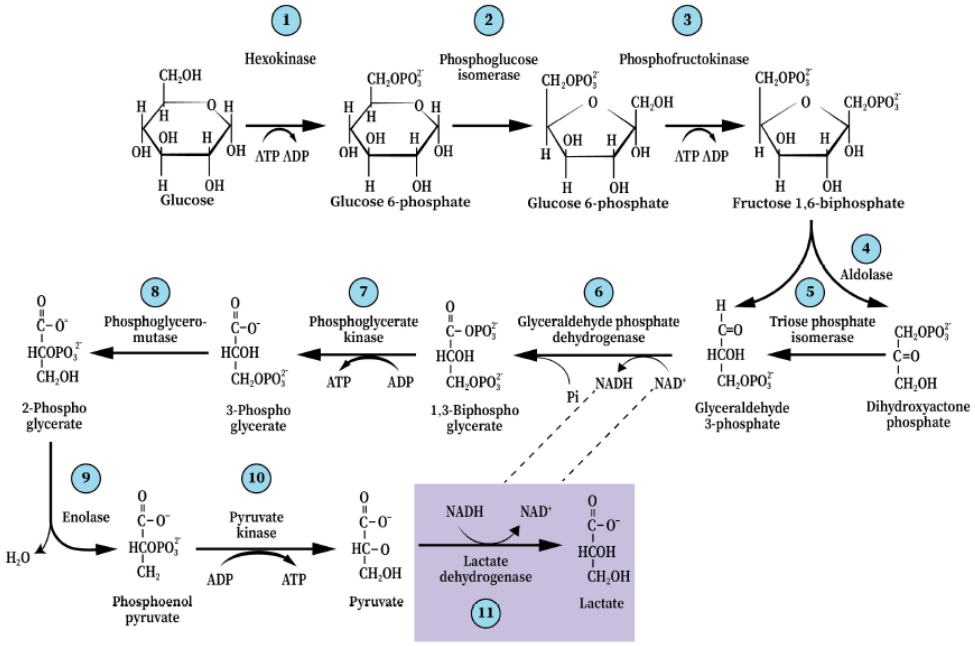

Figure A.1: In this figure different steps of glycolysis in the cytoplasm is shown. Glucose is first phosphorylated and finally is converted to pyruvate. The enzyme for each step is written under the step number. There are reactions in which ATP is produced and reactions with net ATP consumption. Step 11 is where the lactate is produced from pyruvate. This scheme is taken from [4].

Bibliography

[1] P. J. Magistretti and I. Allaman, "Lactate in the brain: from metabolic end-product to signalling molecule," *Nature Reviews Neuroscience*, vol. 19, no. 4, pp. 235–249, 2018.

[2] F. Baeza-Lehnert, A. S. Saab, R. Gutiérrez, V. Larenas, E. Díaz, M. Horn, M. Vargas, L. Hösli, J. Stobart, J. Hirrlinger, B. Weber, and L. F. Barros, "Non-canonical control of neuronal energy status by the na+ pump," *Cell Metabolism*, vol. 29, no. 3, pp. 668–680.e4, 2019.

[3] C. M. Díaz-García and G. Yellen, "Neurons rely on glucose rather than astrocytic lactate during stimulation," *Journal of Neuroscience Research*, vol. 97, no. 8, pp. 883–889, 2019.

[4] A. Schurr, "Glycolysis paradigm shift dictates a reevaluation of glucose and oxygen metabolic rates of activated neural tissue," *Front Neurosci*, vol. 12, p. 700, 2018.

[5] A. Gjedde, W. Bauer, and D. Wong, *Neurokinetics: The dynamics of neurobiology in vivo*. Springer US, 2011.

[6] A. Schurr and e. Gozal, "Aerobic production and utilization of lactate satisfy increased energy demands upon neuronal activation in hippocampal slices and provide neuroprotection against oxidative stress," *Frontiers in Pharmacology*, vol. 2, no. 96, 2012.

[7] E. R. Kandel, *Principles of neural science*, 2013.

[8] N. J. Allen and C. Eroglu, "Cell biology of astrocyte-synapse interactions," *Neuron*, vol. 96, no. 3, pp. 697–708, 2017.

[9] G. C. Rangel, "Computational predictive modeling of integrated cerebral metabolism,

electrophysiology and hemodynamics," Thesis, 2019. [Online]. Available: http://hdl.handle.net/10810/32544

[10] S. N. Vaishnavi, A. G. Vlassenko, M. M. Rundle, A. Z. Snyder, M. A. Mintun, and M. E. Raichle, "Regional aerobic glycolysis in the human brain," *Proceedings of the National Academy of Sciences*, vol. 107, no. 41, p. 17757, 2010.

[11] E. Somersalo, Y. Cheng, and D. Calvetti, "The metabolism of neurons and astrocytes through mathematical models," *Annals of Biomedical Engineering*, vol. 40, no. 11, pp. 2328–2344, 2012.

[12] J.-Y. Chatton, L. Pellerin, and P. J. Magistretti, "Gaba uptake into astrocytes is not associated with significant metabolic cost: Implications for brain imaging of inhibitory transmission," *Proceedings of the National Academy of Sciences*, vol. 100, no. 21, p. 12456, 2003.

[13] A. Suzuki, S. A. Stern, O. Bozdagi, G. W. Huntley, R. H. Walker, P. J. Magistretti, and C. M. Alberini, "Astrocyte-neuron lactate transport is required for long-term memory formation," *Cell*, vol. 144, no. 5, pp. 810–23, 2011.

[14] N. Sada, S. Lee, T. Katsu, T. Otsuki, and T. Inoue, "Epilepsy treatment. targeting ldh enzymes with a stiripentol analog to treat epilepsy," *Science*, vol. 347, no. 6228, pp. 1362–7, 2015.

[15] M. T. Wyss, R. Jolivet, A. Buck, P. J. Magistretti, and B. Weber, "¡em¿in vivo¡/em¿ evidence for lactate as a neuronal energy source," *The Journal of Neuroscience*, vol. 31, no. 20, pp. 7477–7485, 2011.

[16] G. A. Dienel, "Brain lactate metabolism: the discoveries and the controversies," *Journal of cerebral blood flow and metabolism*, vol. 32, no. 7, pp. 1107–1138, 2012.

[17] L. Pellerin and P. J. Magistretti, "Glutamate uptake into astrocytes stimulates aerobic glycolysis: a mechanism coupling neuronal activity to glucose utilization," vol. 91, no. 22, pp. 10 625–10 629, 1994.

[18] L. Pellerin, G. Pellegri, P. G. Bittar, Y. Charnay, C. Bouras, J. L. Martin, N. Stella, and P. J.

Magistretti, “Evidence supporting the existence of an activity-dependent astrocyte-neuron lactate shuttle,” *Dev Neurosci*, vol. 20, no. 4-5, pp. 291–9, 1998.

[19] D. Boison and C. Steinhäuser, “Epilepsy and astrocyte energy metabolism,” *Glia*, vol. 66, no. 6, pp. 1235–1243, 2018.

[20] T. Matsui, H. Omuro, Y.-F. Liu, M. Soya, T. Shima, B. S. McEwen, and H. Soya, “Astrocytic glycogen-derived lactate fuels the brain during exhaustive exercise to maintain endurance capacity,” *Proceedings of the National Academy of Sciences*, vol. 114, no. 24, p. 6358, 2017.

[21] P. Rasmussen, M. T. Wyss, and C. Lundby, “Cerebral glucose and lactate consumption during cerebral activation by physical activity in humans,” *The FASEB Journal*, vol. 25, no. 9, pp. 2865–2873, 2011.

[22] B. Quistorff, N. H. Secher, and J. J. Van Lieshout, “Lactate fuels the human brain during exercise,” *The FASEB Journal*, vol. 22, no. 10, pp. 3443–3449, 2008.

[23] V. Mosienko, A. G. Teschemacher, and S. Kasparov, “Is l-lactate a novel signaling molecule in the brain?” *Journal of Cerebral Blood Flow and Metabolism*, vol. 35, no. 7, pp. 1069–1075, 2015.

[24] A. P. Halestrap, “The monocarboxylate transporter family—structure and functional characterization,” *IUBMB Life*, vol. 64, no. 1, pp. 1–9, 2012.

[25] K. Pierre and L. Pellerin, “Monocarboxylate transporters in the central nervous system: distribution, regulation and function,” vol. 94, no. 1, pp. 1–14, 2005.

[26] L. H. Bergersen, “Is lactate food for neurons? comparison of monocarboxylate transporter subtypes in brain and muscle,” *Neuroscience*, vol. 145, no. 1, pp. 11–19, 2007.

[27] L. Hertz, “The astrocyte-neuron lactate shuttle: A challenge of a challenge,” *Journal of Cerebral Blood Flow and Metabolism*, vol. 24, no. 11, pp. 1241–1248, 2004.

[28] F. Lauritzen, T. Eid, and L. H. Bergersen, “Monocarboxylate transporters in temporal lobe epilepsy: roles of lactate and ketogenic diet,” *Brain Structure and Function*, vol. 220, no. 1, pp. 1–12, 2015.

[29] N. Vijay and M. E. Morris, "Role of monocarboxylate transporters in drug delivery to the brain," *Current pharmaceutical design*, vol. 20, no. 10, pp. 1487–1498, 2014.

[30] L. Hertz, M. E. Gibbs, and G. A. Dienel, "Fluxes of lactate into, from, and among gap junction-coupled astrocytes and their interaction with noradrenaline," *Front Neurosci*, vol. 8, p. 261, 2014.

[31] A. Beland-Millar, J. Larcher, J. Courtemanche, T. Yuan, and C. Messier, "Effects of systemic metabolic fuels on glucose and lactate levels in the brain extracellular compartment of the mouse," *Front Neurosci*, vol. 11, p. 7, 2017.

[32] B. G. Ramírez, T. B. Rodrigues, I. R. Violante, F. Cruz, L. L. Fonseca, P. Ballesteros, M. M. C. A. Castro, M. L. García-Martín, and S. Cerdán, "Kinetic properties of the redox switch/redox coupling mechanism as determined in primary cultures of cortical neurons and astrocytes from rat brain," *Journal of Neuroscience Research*, vol. 85, no. 15, pp. 3244–3253, 2007.

[33] L. B. Gladden, "Lactate metabolism: a new paradigm for the third millennium," vol. 558, no. 1, pp. 5–30, 2004.

[34] T. Sotelo-Hitschfeld, M. I. Niemeyer, P. Machler, I. Ruminot, R. Lerchundi, M. T. Wyss, J. Stobart, I. Fernandez-Moncada, R. Valdebenito, P. Garrido-Gerter, Y. Contreras-Baeza, B. L. Schneider, P. Aebischer, S. Lengacher, A. San Martin, J. Le Douce, G. Bonvento, P. J. Magistretti, F. V. Sepulveda, B. Weber, and L. F. Barros, "Channel-mediated lactate release by k(+)-stimulated astrocytes," *J Neurosci*, vol. 35, no. 10, pp. 4168–78, 2015.

[35] P. Machler, M. T. Wyss, M. Elsayed, J. Stobart, R. Gutierrez, A. von Faber-Castell, V. Kaelin, M. Zuend, A. San Martin, I. Romero-Gomez, F. Baeza-Lehnert, S. Lengacher, B. L. Schneider, P. Aebischer, P. J. Magistretti, L. F. Barros, and B. Weber, "In vivo evidence for a lactate gradient from astrocytes to neurons," *Cell Metab*, vol. 23, no. 1, pp. 94–102, 2016.

[36] A. Schurr and R. S. Payne, "Lactate, not pyruvate, is neuronal aerobic glycolysis end product: An in vitro electrophysiological study," *Neuroscience*, vol. 147, no. 3, pp. 613–619, 2007.

[37] I. A. Simpson, A. Carruthers, and S. J. Vannucci, "Supply and demand in cerebral energy metabolism: the role of nutrient transporters," *Journal of cerebral blood flow and metabolism*, vol. 27, no. 11, pp. 1766–1791, 2007.

[38] S. Mangia, I. A. Simpson, S. J. Vannucci, and A. Carruthers, "The in vivo neuron-to-astrocyte lactate shuttle in human brain: evidence from modeling of measured lactate levels during visual stimulation," vol. 109, no. s1, pp. 55–62, 2009.

[39] M. A. Castro, F. A. Beltrán, S. Brauchi, and I. I. Concha, "A metabolic switch in brain: glucose and lactate metabolism modulation by ascorbic acid," vol. 110, no. 2, pp. 423–440, 2009.

[40] T. Takata, B. Yang, T. Sakurai, Y. Okada, and K. Yokono, "Glycolysis regulates the induction of lactate utilization for synaptic potentials after hypoxia in the granule cell of guinea pig hippocampus," *Neuroscience Research*, vol. 50, no. 4, pp. 467–474, 2004.

[41] L. Pellerin, "Brain energetics (thought needs food)," vol. 11, no. 6, pp. 701–705, 2008.

[42] G. A. Brooks, "The science and translation of lactate shuttle theory," *Cell Metab*, vol. 27, no. 4, pp. 757–785, 2018.

[43] A. Schurr, "Cerebral glycolysis: a century of persistent misunderstanding and misconception," *Front Neurosci*, vol. 8, p. 360, 2014.

[44] E. Vendel, V. Rottschäfer, and E. C. M. de Lange, "The need for mathematical modelling of spatial drug distribution within the brain," *Fluids and Barriers of the CNS*, vol. 16, no. 1, p. 12, 2019.

[45] S. Blanchard, S. Saillet, A. Ivanov, P. Benquet, C.-G. Bénar, M. Pélégrini-Issac, H. Benali, and F. Wendling, "A new computational model for neuro-glio-vascular coupling: Astrocyte activation can explain cerebral blood flow nonlinear response to interictal events," *PLOS ONE*, vol. 11, no. 2, pp. 1–21, 02 2016.

[46] B. P. Ingalls, *Mathematical modeling in systems biology : an introduction*. MIT Press, 2013.

[47] "Transport and Kinetics," 3 2021, [Online; accessed 2021-10-12]. [Online]. Available: https://bio.libretexts.org/@go/page/4534

[48] J. Keener, *Mathematical physiology*. Springer, 2014.

[49] A. Aubert, R. Costalat, P. J. Magistretti, and L. Pellerin, "Brain lactate kinetics: Modeling evidence for neuronal lactate uptake upon activation," *Proceedings of the National Academy of Sciences of the United States of America*, vol. 102, no. 45, p. 16448, 2005.

[50] A. Aubert and R. Costalat, "A model of the coupling between brain electrical activity, metabolism, and hemodynamics: Application to the interpretation of functional neuroimaging," *NeuroImage*, vol. 17, no. 3, pp. 1162–1181, 2002.

[51] ——, "Interaction between astrocytes and neurons studied using a mathematical model of compartmentalized energy metabolism," *J Cereb Blood Flow Metab*, vol. 25, no. 11, pp. 1476–90, 2005.

[52] Y. Hu and G. S. Wilson, "A temporary local energy pool coupled to neuronal activity: Fluctuations of extracellular lactate levels in rat brain monitored with rapid-response enzyme-based sensor," *Journal of Neurochemistry*, vol. 69, no. 4, pp. 1484–1490, 1997.

[53] R. Jolivet, I. Allaman, L. Pellerin, P. J. Magistretti, and B. Weber, "Comment on recent modeling studies of astrocyte–neuron metabolic interactions," *Journal of Cerebral Blood Flow and Metabolism*, vol. 30, no. 12, pp. 1982–1986, 2010.

[54] S. Mangia, M. DiNuzzo, F. Giove, A. Carruthers, I. A. Simpson, and S. J. Vannucci, "Response to 'comment on recent modeling studies of astrocyte—neuron metabolic interactions': Much ado about nothing," *Journal of Cerebral Blood Flow and Metabolism*, vol. 31, no. 6, pp. 1346–1353, 2011.

[55] D. Calvetti, Y. Cheng, and E. Somersalo, "Uncertainty quantification in flux balance analysis of spatially lumped and distributed models of neuron–astrocyte metabolism," *Journal of Mathematical Biology*, vol. 73, no. 6, pp. 1823–1849, 2016.

[56] M. Cloutier, F. B. Bolger, J. P. Lowry, and P. Wellstead, "An integrative dynamic model of brain energy metabolism using in vivo neurochemical measurements," *Journal of Computational Neuroscience*, vol. 27, no. 3, p. 391, 2009.

[57] G. Capo Rangel, J. Prezioso, L. Gerardo-Giorda, E. Somersalo, and D. Calvetti, "Brain energetics plays a key role in the coordination of electrophysiology, metabolism and hemodynamics: Evidence from an integrated computational model," *Journal of Theoretical Biology*, vol. 478, pp. 26–39, 2019.

[58] D. Calvetti and E. Somersalo, "Dynamic activation model for a glutamatergic neurovascular unit," *Journal of Theoretical Biology*, vol. 274, no. 1, pp. 12–29, 2011.

[59] D. G. Patsatzis, E.-A. Tingas, D. A. Goussis, and S. M. Sarathy, "Computational singular perturbation analysis of brain lactate metabolism," *PLOS ONE*, vol. 14, no. 12, pp. 1–37, 12 2019.

[60] R. Jolivet, J. S. Coggan, I. Allaman, and P. J. Magistretti, "Multi-timescale modeling of activity-dependent metabolic coupling in the neuron-glia-vasculature ensemble," *PLOS Computational Biology*, vol. 11, no. 2, p. e1004036, 2015.

[61] K. L. Du and M. N. S. Swamy, *Search and Optimization by Metaheuristics*. Springer, 2016.

[62] F. Reali, C. Priami, and L. Marchetti, "Optimization algorithms for computational systems biology," *Frontiers in Applied Mathematics and Statistics*, vol. 3, p. 6, 2017.

[63] "Matlab global optimization toolbox: User's guide," 2019, the MathWorks, Natick, MA, USA.

[64] E. Atashpaz-Gargari and C. Lucas, "Imperialist competitive algorithm: An algorithm for optimization inspired by imperialistic competition," in *2007 IEEE Congress on Evolutionary Computation*, 2007, pp. 4661–4667.

[65] M. Abdollahi, A. Isazadeh, and D. Abdollahi, "Imperialist competitive algorithm for solving systems of nonlinear equations," *Computers & Mathematics with Applications*, vol. 65, no. 12, pp. 1894 – 1908, 2013.

[66] M. Emmerich and A. A. Deutz, "A tutorial on multiobjective optimization: fundamentals and evolutionary methods," *Nat Comput*, vol. 17, p. 585–609, 2018.

[67] L. F. Barros, C. X. Bittner, A. Loaiza, and O. H. Porras, "A quantitative overview of glucose dynamics in the gliovascular unit," *Glia*, vol. 55, no. 12, pp. 1222–1237, 2007.

[68] P. Jukkola and C. Gu, "Regulation of neurovascular coupling in autoimmunity to water and ion channels," *Autoimmunity Reviews*, vol. 14, no. 3, pp. 258–267, 2015.

[69] J. E. Cremer, V. J. Cunningham, W. M. Pardridge, L. D. Braun, and W. H. Oldendorf, "Kinetics of blood-brain barrier transport of pyruvate, lactate and glucose in suckling, weanling and adult rats," *Journal of Neurochemistry*, vol. 33, no. 2, pp. 439–445, 1979, https://doi.org/10.1111/j.1471-4159.1979.tb05173.x. [Online]. Available: https://doi.org/10.1111/j.1471-4159.1979.tb05173.x

[70] W. G. Kuhr, C. J. van den Berg, and J. Korf, "In vivo identification and quantitative evaluation of carrier-mediated transport of lactate at the cellular level in the striatum of conscious, freely moving rats," *Journal of Cerebral Blood Flow and Metabolism*, vol. 8, no. 6, pp. 848–856, 1988. [Online]. Available: https://doi.org/10.1038/jcbfm.1988.142

[71] G. K. Gandhi, N. F. Cruz, K. K. Ball, and G. A. Dienel, "Astrocytes are poised for lactate trafficking and release from activated brain and for supply of glucose to neurons," vol. 111, no. 2, pp. 522–536, 2009.

[72] K. S. Dimmer, B. Friedrich, F. Lang, J. W. Deitmer, and S. Bröer, "The low-affinity monocarboxylate transporter mct4 is adapted to the export of lactate in highly glycolytic cells," *The Biochemical journal*, vol. 350 Pt 1, no. Pt 1, pp. 219–227, 2000.

[73] S. Sasaki, M. Kobayashi, Y. Futagi, J. Ogura, H. Yamaguchi, N. Takahashi, and K. Iseki, "Crucial residue involved in l-lactate recognition by human monocarboxylate transporter 4 (hmct4)," *PloS one*, vol. 8, no. 7, pp. e67 690–e67 690, 2013.

[74] J. C. LaManna, J. Frederick Harrington, L. M. Vendel, K. Abi-Saleh, W. David Lust, and S. I. Harik, "Regional blood-brain lactate influx," *Brain Research*, vol. 614, no. 1, pp. 164–170, 1993.

[75] J. O'Brien, K. M. Kla, I. B. Hopkins, E. A. Malecki, and M. C. McKenna, "Kinetic parameters and lactate dehydrogenase isozyme activities support possible lactate utilization by neurons," *Neurochemical Research*, vol. 32, no. 4, pp. 597–607, 2007. [Online]. Available: https://doi.org/10.1007/s11064-006-9132-9

[76] A. Atlante, L. de Bari, A. Bobba, E. Marra, and S. Passarella, "Transport and metabolism of l-lactate occur in mitochondria from cerebellar granule cells and are modified in cells undergoing low potassium dependent apoptosis," *Biochimica et Biophysica Acta (BBA) - Bioenergetics*, vol. 1767, no. 11, pp. 1285–1299, 2007. [Online]. Available: https://www.sciencedirect.com/science/article/pii/S0005272807001958

[77] A. Gjedde and S. Marrett, "Glycolysis in neurons, not astrocytes, delays oxidative metabolism of human visual cortex during sustained checkerboard stimulation in vivo," 2001.

[78] L. C. Felippe, G. A. Ferreira, F. De-Oliveira, F. O. Pires, and A. E. Lima-Silva, "Arterialized and venous blood lactate concentration difference during different exercise intensities," *Journal of Exercise Science and Fitness*, vol. 15, no. 1, pp. 22–26, 2017.

[79] I. Ruminot, J. Schmälzle, B. Leyton, L. F. Barros, and J. W. Deitmer, "Tight coupling of astrocyte energy metabolism to synaptic activity revealed by genetically encoded fret nanosensors in hippocampal tissue," *Journal of Cerebral Blood Flow and Metabolism*, vol. 39, no. 3, pp. 513–523, 2017.

[80] A. San Martín, S. Ceballo, I. Ruminot, R. Lerchundi, W. B. Frommer, and L. F. Barros, "A genetically encoded fret lactate sensor and its use to detect the warburg effect in single cancer cells," *PLOS ONE*, vol. 8, no. 2, p. e57712, 2013.

[81] G. Qian and A. Mahdi, "Sensitivity analysis methods in the biomedical sciences," *Mathematical Biosciences*, vol. 323, p. 108306, 2020. [Online]. Available: https://www.sciencedirect.com/science/article/pii/S0025556420300018